Organic & Biomolecular Chemistry

Accepted Manuscript

ROYAL SOCIETY OF CHEMISTRY

rsc.li/obc

View Article Online
DOI: 10.1039/C7OB02045G

Rational design and structure-activity relationship studies of quercetin-amino acid hybrids targeting the anti-apoptotic protein Bcl-xL

Tahsin F. Kellici[a,b], *Maria V. Chatziathanasiadou*[a], *Min-Sung Lee*[c], *Nisar Sayyad*[a], Geromichalou EG[d], *Eirinaios I. Vrettos*[a], *Antonis D. Tsiailanis*[a], *Seung-Wook Chi*[c], George D Geromichalos[e,f] *Thomas Mavromoustakos*[b], *Andreas G. Tzakos*[a,]*

[a]Department of Chemistry, University of Ioannina, Ioannina 45110, Greece

[b]Department of Chemistry, National and Kapodistrian University of Athens, Panepistimiopolis Zografou 15771, Greece

[c]Disease Target Structure Research Center, KRIBB, Daejeon 34141, Republic of Korea

[d]Laboratory of Pharmacology, Medical School National and Kapodistrian University of Athens, Athens 11527, Greece

[e]Laboratory of Inorganic Chemistry, Faculty of Chemistry, Aristotle University of Thessaloniki, GR-54124 Thessaloniki, Greece

[f]Cell Culture, Molecular Modelling and Drug Design Lab., Symeonidion Research Center, Theagenion Cancer Hospital, Thessaloniki, Greece

Corresponding Authors

* Tel.: +3026510 08387, E-mail: agtzakos@gmail.com (A. Tzakos)

View Article Online
DOI: 10.1039/C7OB02045G

Abstract

Anti-apoptotic proteins, like the Bcl-2 family proteins, present an important therapeutic cancer drug target. Their activity is orchestrated through neutralization upon interaction of pro-apoptotic protein counterparts that leads to immortality of cancer cells. Therefore, generating compounds targeting these proteins is of immense therapeutic importance. Herein, Induced Fit Docking (IFD) and Molecular Dynamics (MD) simulations were performed to rationally design quercetin analogues that bind in the BH3 site of the Bcl-xL protein. IFD calculations determined their binding cavity while Molecular Mechanics Poisson Boltzmann Surface Area (MM-PBSA) and Molecular Mechanics Generalised Born Surface Area (MM-GBSA) calculations provided an insight into the binding enthalpies of the analogues. The quercetin analogues were synthesized and their binding to Bcl-xL was verified with fluorescence spectroscopy. The binding affinity and the thermodynamic parameters between Bcl-xL and quercetin-glutamic acid were estimated through Isothermal Titration Calorimetry. 2D $^{1}H–^{15}N$ HSQC NMR chemical shift perturbation mapping was used to map the binding site of the quercetin analogues in the Bcl-xL that overlapped with the predicted poses generated by both IFD and MD calculations. Furthermore, evaluation of the four conjugates against the prostate DU-145 and PC-3 cancer cell lines, revealed quercetin-glutamic acid and quercetin-alanine as the most potent conjugates bearing the higher cytostatic activity. This pinpoints that the chemical space of natural products can be tailored to exploit new hits for difficult tractable targets such as protein-protein interactions.

Keywords: Bcl-xL; Quercetin analogues; Induced fit docking; Molecular Dynamics; Protein-protein interactions; fluorescence spectroscopy; 2D HSQC NMR

View Article Online
DOI: 10.1039/C7OB02045G

Introduction

Programmed cell death (apoptosis) plays a pivotal role in the normal growth, homeostasis of tissues and removal of infected or dangerous cells. The alteration of apoptosis results in the occurrence of different diseases such as inflammation, tumor development, tumor cell resistance to chemotherapy, neoplasia, neurodegeneration or autoimmune disorders. As a result, the molecular mechanisms responsible for the apoptotic cell death are highly conserved [1-4].

It is now well-established that the B-cell lymphoma-2 family proteins directly regulate all major types of cell death, including necrosis, autophagy and apoptosis [5]. This family is subdivided into the anti-apoptotic proteins (i.e. Bcl-2, Bcl-xL, Bcl-W, Mcl-1 and A1) and the pro-apoptotic proteins (i.e. Bax, Bak, Bad, Bim, PUMA, Noxa)[1,6]. Bcl-xL binds the proapoptotic proteins Bax and Bak in the third B-cell homology domain (BH3), antagonizing cell apoptosis [7-10]. The X-ray structure of Bcl-xL with the BH3 domain of Bad and Bim provided a basis for the rationalization of the binding mode of these pro-apoptotic proteins to the hydrophobic groove of Bcl-xL [11, 12]. Bcl-xL is comprised of eight α-helices connected by loops of different lengths [4]. The homology domains BH1, BH2 and BH3 form a hydrophobic cavity in the surface of the protein. This cleft is the binding site of the BH3 domains of the proapoptotic proteins and the main target for small molecules acting as inhibitors of these protein-protein interactions (PPI)[13]. The BH3 inhibitor WEHI-539 induces a significant conformational change around the p2 pocket to accommodate their benzothiazole moiety. It was suggested that WEHI-539's selectivity for Bcl-xL may be due to an array of hydrogen bonds taking place in this enlarged p2 pocket between the benzothiazole hydrazone group and backbone NH and carbonyls. The hydrophobic compound ABT-737 binds in two out of four key hydrophobic pockets on the surface of their pro-survival protein targets (p2 and p4) inducing an important remodeling of the p2 pocket[14].

The interface implicated in protein-protein interactions is flat and extensive and thus triggers a special challenge in developing small molecules targeting this biological space[15, 16]

View Article Online
DOI: 10.1039/C7OB02045G

[17]. One of the major breakthroughs in this direction was made by the pharmaceutical company Abbott, which disclosed in 2005 ABT-737, a small molecule that binds to Bcl-xL, Bcl-2 and Bcl-W with subnanomolar affinity[16]. This compound has a large molecular weight (813 Da) and presents low oral bioavailability[16]. Recently, the same company disclosed the compounds Navitoclax (ABT-263) [discontinued in phase II clinical trials] and Venetoclax (ABT-199). Finally, on April 2016 Vevetoclax was approved by FDA as a second line treatment of chronic lymphocytic leukemia (CLL). However, this was the only synthetic BH3 mimetic that managed to pass the three phases of clinical trials, whereas many other like Oblimersen, Obatoclax and Navitoclax were rejected[18]. Therefore, the quest to identify novel compounds targeting these therapeutic targets is of importance and the relevant efforts are in the forefront.

Natural products have served as a rich and profitable source for drugs[19]. Our group recently reported that the plant flavonoid quercetin directly binds to the BCL-2 family proteins and triggers their proapoptotic activity[20]. Through this study we unveiled the interaction profile developed by quercetin and the target protein. In our effort to enhance the solubility of the parent compound, quercetin, as also to construct analogues able to develop favorable interactions with the BH3-binding site of Bcl-xL we rationally designed several quercetin hybrids (Figure 1) using Induced Fit Docking (IFD) and Molecular Dynamics (MD) simulations. Our inspiration was based on the fact that cancer cells adopt an increased demand for nutrients and amino acids and selective amino acid transporters have been identified to be upregulated in cancer cells in response to this increased demand [21]. Peptide transporters have been identified to be overexpressed in several tumors and have been characterized as promising targets for tumor-specific drug delivery[22]. Specifically, the human peptide transporter, hPEPT1, has been involved in the transportation of amino acids into the intestine. hPEPT1 has been also implicated to recognize amino acids conjugated to a drug and has thus been exploited to transport drug-amino acid conjugates[23, 24]. Therefore, for drugs with poor permeability, their absorption can be enhanced by attaching to them amino acids and thus recognized and transported by hPEPT1. Along these lines, several different prodrugs based on drug-amino acid conjugates have been reported targeting such receptors allowing enhanced cell permeability profile [25-29]. Given the facts that: (i) quercetin is practically insoluble in aqueous solutions, (ii) we have already charted the interaction architecture of quercetin with BCl-2 family proteins that can be utilized for further rational design of new analogues, (iii) its conjugation with amino acids has amplified the bioavailability of the parent compound [30] and (iv) amino acid transporters are up-regulated in cancer cells, we

View Article Online
DOI: 10.1039/C7OB02045G

rationally designed four quercetin-amino acid conjugates. These conjugates are achieved at 3′ or 4′ positions of quercetin and involve the different degree lipophilic amino acids Ala, Phe, Glu and Leu. In addition, these conjugates are designed to allow increase of multiple interactions contacts in terms of quercetin and therefore increase the binding affinity.

Molecular Mechanics Poisson Boltzmann Surface Area (MM-PBSA) and Molecular Mechanics Generalised Born Surface Area (MM-GBSA) calculations provided an insight into the binding enthalpies of the analogues. The compounds were then synthesized and their binding to Bcl-xL was evaluated with fluorescence spectroscopy and the thermodynamics of the interaction between Bcl-xL and Que-Glu were determined with isothermal titration calorimetry. To experimentally map the Bcl-xL binding surface implicated in the interaction of the different quercetin analogues we conducted chemical shift perturbation mapping through 2D ^{1}H-^{15}N HSQC NMR experiments of the ^{15}N-labeled Bcl-xL. In order to evaluate both the cytostatic and cytotoxic effects of the quercetin conjugates as also the implication on their activity of peptide transporters, we conducted *in vitro* studies in the prostate cancer cell line PC-3, that has been established as a cell culture model for hPEPT1[22], and DU-145 as a negative control.

View Article Online
DOI: 10.1039/C7OB02045G

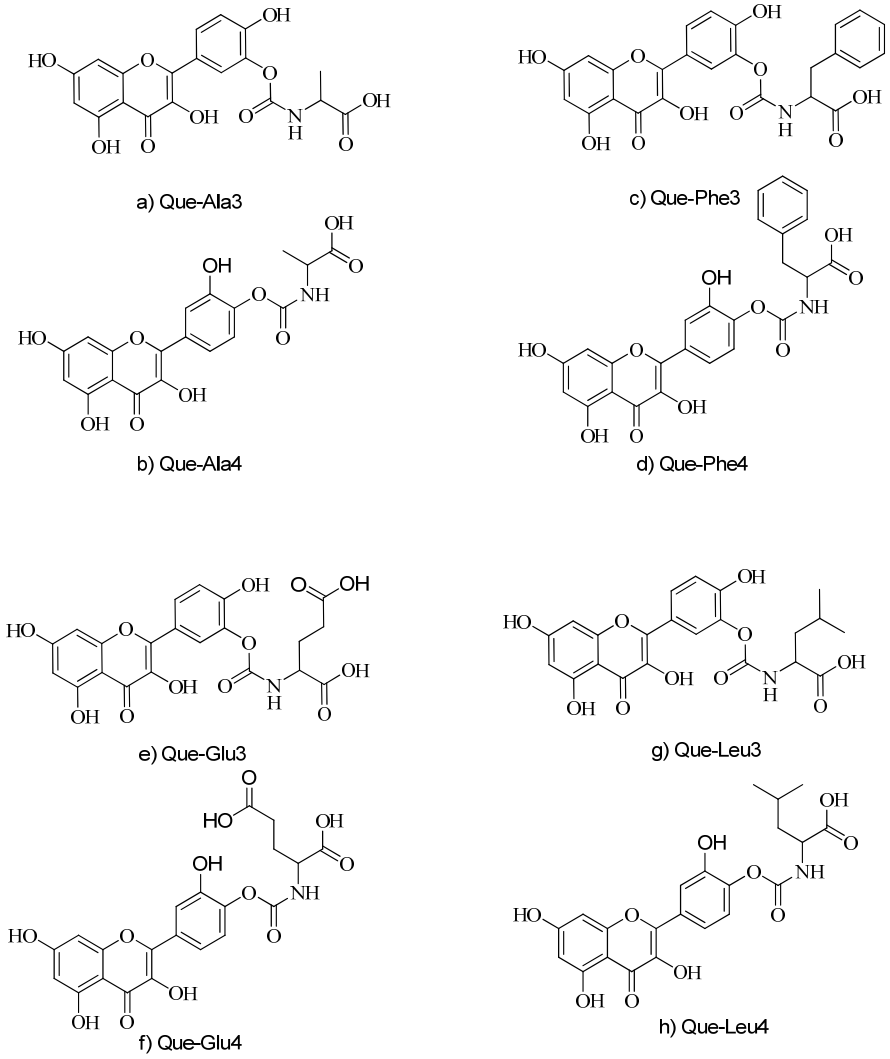

Figure 1: The newly synthesized quercetin analogues as Bcl-xL inhibitors.

Materials and Methods

All chemicals were of the best grade commercially available (Acros Organics, Sigma Aldrich, Alfa-Aesar, Fluka and Merck) and were used without further purification. All solvents were purified according to standard procedures; dry solvents were obtained according to methods previously described in the literature and stored over molecular sieves. HPLC grade acetonitrile and water, purchased from Fischer Scientific, were used for the RP-HPLC. Analytical thin-layer chromatography was performed on glass plates coated with silica gel containing calcium sulfate binder. Column chromatography was performed using SiO_2 and Dichloromethane-Methanol mixtures were used for elution. The ^{1}H NMR and ^{13}C NMR spectra were recorded at 400 MHz in DMSO-d_6 and 298 K. The samples were titrated

View Article Online
DOI: 10.1039/C7OB02045G

with 1 M solution of picric acid in DMSO-d_6 to make the peaks derived from the phenol groups sharper (the peak broadening of these hydroxyl protons is due to rapid intermolecular exchange which is minimized upon addition of picric acid as our group has recently shown[31]). Chemical shifts for ^{1}H NMR spectra are reported as δ units of parts per million (ppm) and relative to the signal of DMSO (δ 2,50 multiplet). Multiplicities are given as follows: s (singlet); d (doublet); dd (doublet of doublets); t (triplet); bs (broad singlet); m (multiplet). Coupling constants are reported as J values in Hz (Supplementary Information 1, 2-1 – 2.8). For the MS analysis, each quercetin derivative was diluted in ACN:H_2O (50:50 v/v) and injected directly to the EVOQ™ Elite ER LC-TQ system (Bruker, Germany). LC-MS grade acetonitrile and water were obtained from Fischer. The analyses were performed using an ESI probe in negative ionization with a spray voltage (-) set to 4000 V. The cone and heated probe temperature were set to 300°C and 25°C, respectively. A nebulizer gas flow equal to 20 units and a cone gas flow of 25 units were applied for the solvent evaporation. MS spectra were collected and analyzed through the MSWS 8.2 software, provided by Bruker.

Preparation of the quercetin - amino acid analogues

The quercetin conjugates were synthesized based on the previous publication by Kim *et al.* [30] with few modifications to successfully enhance the overall yield. Briefly, the addition of DIPEA (2eq) was conducted every day for 3-4 days instead of a single addition and as a result the yield of this step was increased by 10-15% for each conjugate. Reaction was monitored by thin layer chromatography, which indicated that Quercetin as a starting material was completely consumed at the final day. Moreover, the final compounds were obtained via precipitation with hexane instead of recrystallization with acetone/CH_2Cl_2 which resulted in the same yield as reported but in minimum time and effort.

Specifically, amino acids were converted to their tert-butyl esters through reaction with perchloric acid ($HClO_4$) and tert-butyl acetate as a solvent in airtight closed vessel. These tert-butyl esters of amino acids were transformed into their active urethane with the usage of Bis(4-nitrophenyl)carbonate (BNPC) and N,N-Diisopropylethylamine (DIPEA) in anhydrous THF, followed by alcoholysis of quercetin. Final deprotection of the tert-butyl protecting group was achieved by non-aqueous hydrolysis (TFA/CH_2Cl_2), resulting to the expected quercetin-amino acid conjugate and characterization was conducted with NMR, mass and IR spectroscopic techniques (Supplementary Fig. S1-Fig. S13)

View Article Online
DOI: 10.1039/C7OB02045G

Rapid intramolecular transesterification causes the formation of two inseparable regioisomers in a 3:1 ratio[32] (supplementary information) as seen in Figure 1. ^{1}H NMR spectra confirmed these results and showed that the major isomer was the 3'-O-substituted quercetin (a, c) and the minor was 4'-O-substituted quercetin (b, d).

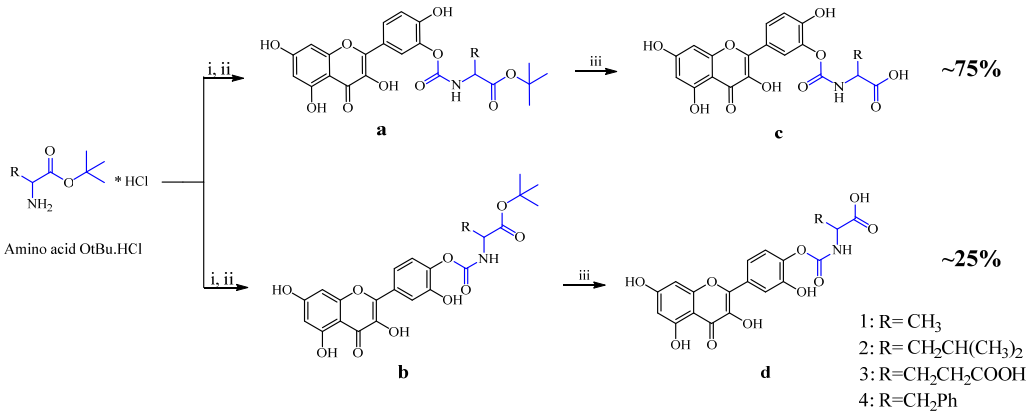

Figure 1: General synthetic scheme for Quercetin-amino acids. i) BNPC, DIPEA, THF, rt, 12h; ii) Quercetin, rt, 12h; iii) TFA/CH_2Cl_2 (1/10, v/v), 0 ^{0}C to rt, 4h.

Synthesis of 3'-O-CO-(Amino acid-OtBu)-Quercetin (a) and 4'-O-CO-(Amino acid-OtBu)-Quercetin (b).

DIPEA (1.1 mmol) was added to the solution of OtBu-amino acid (0.550 mmol) and Bis(4-nitrophenyl)carbonate (0.550 mmol) in anhydrous THF (20 ml) at room temperature under nitrogen atmosphere. After 12 hours, Quercetin (0.550 mmol) was added and the reaction mixture was stirred at room temperature for another 12 hours. DIPEA (1.1 mmol) was being added for 3-4 days until complete consumption of quercetin was verified by TLC. The reaction's solvent was evaporated on rotary evaporator and the crude compound was purified by column chromatography (dichloromethane/methanol, 8:2) to afford inseparable mixture of the regioisomers (a and b) as yellow solid.

NMR and MS characterization of 3'-O-CO-(Ala-OtBu)-Quercetin (1a) and 4'-O-CO-(Ala-OtBu)-Quercetin (1b) (76%).

^{1}H-NMR characterization of **1a** (500 MHz, DMSO-d_6, 25^{o}C): δ = 12.47 (s, 1 H, 5-OH), 10.84 (s, 1 H, 7-OH), 10.40 (s, 1 H, 4'-OH), 9.58 (s,1 H, 3-OH), 8.13 (d, J = 7.3 Hz, 1 H, 8'-NH), 7.94 (dd, J = 8.7 Hz, 2.2 Hz, 1 H, 6'-H), 7.88 (d, J = 2.2 Hz, 1 H, 2'-H), 7.09 (d, J = 8.6 Hz, 1 H, 5'-H), 6.48 (d, J = 2.0 Hz, 1 H, 8-H), 6.23 (d, J = 2.0 Hz, 1 H, 6-H), 4.05- 3.99 (m, 1 H, 9′-H), 1.46 (s, 9 H, 12′-H), 1.35 (d, J = 7.2, 3 H, 13'-H) ppm; ^{13}C-NMR (500 MHz, DMSO-

View Article Online
DOI: 10.1039/C7OB02045G

d_6, 25°C): δ = 177.04 (C4), 172.64 (C10'), 164.87 (C7), 161.51 (C5), 157.04 (C9), 154.54 (C7'), 152.5 (C4'), 146.64 (C2), 126.62 (C6′), 123.79 (C2′), 122.50 (C1'), 117.33 (C5′), 103.86 (C10), 98.91 (C6), 94.22 (C8), 81.34(C11'), 50.97 (C9'), 28.40 (C12'), 17.74 (C13') ppm; ^{1}H-NMR characterization of **1b** (500 MHz, DMSO-d_6, 25°C): δ = 12.41 (s, 1 H, 5-OH), 10.89 (s, 1 H, 7-OH), 10.00 (s, 1 H, 3'-OH), 9.69 (s, 1 H, 3-OH), 8.12 (d, J = 7.3 Hz, 1 H, 8'-NH), 7.81 (d, J = 2.0 Hz, 1 H, 2'-H), 7.61 (dd, J = 8.6, 2.0 Hz, 1 H, 6'-H), 7.18 (d, J = 8.6Hz, 1 H, 5'-H), 6.45 (d, J = 2.0 Hz, 1 H, 8-H), 6.24 (d, J = 2.0 Hz, 1 H, 6-H), 4.05- 3.99 (m, 1 H, 9′-H), 1.46 (s, 9 H, 12′-H), 1.35 (d, J = 7.2 Hz, 3 H, 13'-H) ppm; ^{13}C-NMR (500 MHz, DMSO-d_6, 25°C): δ = 177.02 (C4), 172.64 (C10'), 164.86 (C7), 161.65 (C5), 157.00 (C9), 154.50 (C7'), 150.31 (C3'), 146.32 (C2), 140.77 (C4'), 137.75 (C3), 129.4 (C1'), 124.20 (C5′), 119.24 (C6'), 116.55 (C2′), 103.98 (C10), 98.97 (C6), 94.07 (C8), 81.34 (C11'), 50.97 (C9'), 28.40 (C12'),17.74 (C13') ppm; Mass characterization of **1a** and **1b** regioisomers:

Mass: MS (ESI) m/z: $[M-H]^-$ for $C_{23}H_{23}NO_{10}$: calcd: 473.13, found: 472.1.

NMR and MS characterization of 3'-O-CO-(Leu-OtBu)-Quercetin (2a) and 4'-O-CO-(Leu-OtBu)-Quercetin (2b) (75%):

^{1}H-NMR characterization **2a** (500 MHz, DMSO-d_6, 25°C): δ = 12.47 (s, 1 H, 5-OH), 10.83 (s, 1H, 7-OH), 10.40 (s, 1 H, 4'-OH), 9.57 (s, 1 H, 3-OH), 8.09 (d, J = 7.8 Hz, 1 H, 8'-NH), 7.94 (dd, J = 8.6 Hz, 2.2 Hz, 1 H, 6'-H), 7.88 (d, J = 2.2 Hz, 1 H, 2'-H), 7.08 (d, J = 8.6Hz, 1 H, 5'-H), 6.48 (d, J = 2.0 Hz, 1 H, 8-H), 6.23 (d, J = 2.0 Hz, 1 H, 6-H), 4.01- 3.96 (m, 1 H, 9′-H), 1.82-1.74 (m, 1 H, 14'-H), 1.67-1.60 (m, 1 H, 13'a-H), 1.56-1.52 (m, 1 H, 13′b-H), 1.46 (s, 9 H, 12'H), 0.93 (d, J = 6.5, 6 H, 15'H) ppm; ^{13}C-NMR (500 MHz, DMSO-d_6, 25°C): δ = 176.7 (C4), 172.5 (C10'), 164.75 (C7), 161.62 (C5), 156.95 (C9), 154.80 (C7'), 152.63 (C4'), 146.58 (C2), 139.90 (C3'), 132.45 (C3), 126.63 (C6'), 123.63 (C2′), 122.62 (C1'), 117.26 (C5′), 103.86 (C10), 99.09 (C6), 94.21 (C8), 81.49 (C11'), 53.89 (C9'), 40.47 (C13'), 28.50 (C12'), 24.96 (C14'), 22.09 (C15') ppm.

^{1}H-NMR characterization **2b** (500 MHz, DMSO-d_6, 25°C): δ = 12.41 (s, 1 H, 5-OH), 10.89 (s, 1 H, 7-OH), 10.00 (s, 1 H, 3'-OH), 9.68 (s, 1 H, 3-OH), 8.10 (d, J = 7.8 Hz, 1 H, 8'-NH), 7.81 (d, J = 2.2 Hz, 1 H, 2'-H), 7.61 (dd, J = 8.6Hz, 2.2 Hz, 1 H, 6'-H), 7.18 (d, J = 8.6Hz, 1 H, 5'-H), 6.45 (d, J = 2.0 Hz, 1 H, 8-H), 6.24 (d, J = 2.0 Hz, 1 H, 6-H), 4.01- 3.96 (m, 1 H, 9′-H), 1.82-1.74 (m, 1 H, 14'-H), 1.67-1.60 (m, 1 H, 13'a-H), 1.56-1.52 (m, 1 H, 13′b-H), 1.46 (s, 9 H, 12'H), 0.93 (d, J = 6.5, 6 H, 15'H) ppm; ^{13}C-NMR (500 MHz, DMSO-d_6, 25°C): δ = 172.50 (C10'), 164.93 (C7), 161.73 (C5), 154.80 (C7'), 157.09 (C9), 150.31 (C3'),

View Article Online
DOI: 10.1039/C7OB02045G

146.20 (C2), 141.00 (C4'), 122.62 (C1'), 119.34 (C6′), 117.26 (C5′), 116.56 (C2'), 103.90 (C10), 99.19 (C6), 94.06 (C8), 81.49 (C11'), 53.89 (C9'), 40.47 (C13'), 28.50 (C12'), 24.96 (C14'), 22.09 (C15') ppm. Mass characterization of **2a** and **2b** regioisomers:

Mass: MS (ESI) m/z: $[M-H]^-$ for $C_{26}H_{29}NO_{10}$: calcd: 515.18; found: 514.2.

NMR and MS characterization of 3'-O-CO-(Glu-OtBu)-Quercetin (3a) and 4'-O-CO-(Glu-OtBu)-Quercetin (3b) (71%):

^{1}H-NMR characterization **3a** (500 MHz, DMSO-d_6, 25°C): δ = 12.47 (s, 1 H, 5-OH), 10.84 (s, 1 H, 7-OH), 10.36 (s, 1 H, 4'-OH), 9.55 (s, 1 H, 3-OH), 8.11 (d, J = 7.5 Hz, 1 H, 8'-NH), 7.95 (dd, J = 8.6 Hz, 2.2 Hz, 1 H, 6'-H), 7.8 (d, J = 2.2 Hz, 1 H, 2'-H), 7.09 (d, J = 8.6Hz, 1 H, 5'-H), 6.48 (d, J = 2.0 Hz, 1 H, 8-H), 6.23 (d, J = 2.0 Hz, 1 H, 6-H), 4.04- 3.99 (m, 1 H, 9′-H), 2.00 (m, 2 H, 14'-H), 1.87 (m, 2 H, 13'-H), 1.47 (s, 9 H, 17′-H), 1.45 (s, 9 H, 12'-H) ppm; ^{13}C-NMR (500 MHz, DMSO-d_6, 25°C): δ = 176.81 (C4), 172.31 (C15'), 172.31 (C10'), 164.80 (C7), 161.60 (C5), 157.00 (C9), 154.75 (C7'), 152.44 (C4'), 146.59 (C2), 139.59 (C3'), 126.72 (C6′), 123.73 (C2′), 122.63 (C1'), 117.30 (C5′), 103.92 (C10), 98.96 (C6), 94.25 (C8), 81.7 (C11'), 80.72 (C16'), 54.62 (C9'), 28.48 (C17'), 28.48 (C12'), 27.00 (C14'), 27.00 (C13') ppm.

^{1}H-NMR characterization **3b** (500 MHz, DMSO-d_6, 25°C): δ = 12.41 (s, 1 H, 5-OH), 10.88 (s, 1 H, 7-OH), 9.97 (s, 1 H, 3'-OH), 9.68 (s, 1 H, 3-OH), 8.11 (d, J = 7.5 Hz, 1 H, 8'-NH), 7.81 (d, J = 2.2 Hz, 1 H, 2'-H), 7.62 (dd, J = 8.6, 2.2 Hz, 1 H, 6'-H), 7.18 (d, J = 8.6Hz, 1 H, 5'-H), 6.45 (d, J = 2.0 Hz, 1 H, 8-H), 6.24 (d, J = 2.0 Hz, 1 H, 6-H), 4.04- 3.99 (m, 1 H, 9′-H), 2.00 (m, 2 H, 14'-H), 1.87 (m, 2 H, 13'-H), 1.47 (s, 9 H, 17′-H), 1.45 (s, 9 H, 12'-H) ppm; ^{13}C-NMR (500 MHz, DMSO-d_6, 25°C): δ = 177.03 (C4), 172.31 (C10'), 172.30 (C15'), 164.80 (C7), 161.60 (C5), 157.00 (C9), 154.75 (C7'), 150.21 (C3'), 146.36 (C2), 140.86 (C4'), 129.55 (C1′), 124.15 (C5′), 119.33 (C6'), 116.61 (C2′), 103.92 (C10), 98.96 (C6), 94.14 (C8), 81.70 (C11'), 80.72 (C16'), 54.62 (C9'), 28.48 (C17'), 28.48 (C12'), 27.05 (C14'), 27.05 (C13') ppm. Mass characterization of **3a** and **3b** regioisomers: **Mass:** MS (ESI) m/z: $[M-H]^-$ for $C_{29}H_{33}NO_{12}$: calcd: 587.20; found: 586.3.

NMR and MS characterization 4'-O-CO-(Phe-OtBu)-Quercetin (4a) and 4'-O-CO-(Phe-OtBu)-Quercetin (4b) (67%):

View Article Online
DOI: 10.1039/C7OB02045G

^{1}H-NMR characterization **4a** (500 MHz, DMSO-d_6, 25^{o}C): δ = 12.47 (s, 1 H, 5-OH), 10.84 (s, 1H, 7-OH), 10.39 (s, 1 H, 4'-OH), 9.57 (s, 1 H, 3-OH), 8.20 (d, J = 7.7 Hz, 1 H, 8'-NH), 7.93 (dd, J = 8.7 Hz, 2.2 Hz, 1 H, 6'-H), 7.82 (d, J = 2.2 Hz, 1 H, 2'-H), 7.36-7.34 (m, 4 H, 15' and 16'-H), 7.30-7.26 (m, 1 H, 17'-H), 7.08 (d, J = 8.7Hz, 1 H, 5'-H), 6.48 (d, J = 2.0 Hz, 1 H, 8-H), 6.23 (d, J = 2.0 Hz, 1 H, 6-H), 4.22- 4.17 (m, 1 H, 9´-H), 3.08-2.98 (m, 2 H, 13'-H), 1.39 (s, 9 H, 12'-H) ppm; ^{13}C-NMR (500 MHz, DMSO-d_6, 25^{o}C): δ = 176.81 (C4), 171.42 (C10'), 164.76 (C7), 161.63 (C5), 156.98 (C9), 154.59 (C7'), 152.45 (C4'), 146.56 (C2), 139.54 (C3'), 138.2 (C14'), 136.89 (C3), 130.03 (C15'), 129.05 (C16'), 127.32 (C17'), 126.69 (C6'), 123.69 (C2´), 122.45 (C1'), 117.25 (C5´), 103.91 (C10), 98.98 (C6), 94.25 (C8), 81.66 (C11'), 57.08 (C9'), 37.56 (C13'), 28.43 (C12') ppm.

^{1}H-NMR characterization **4b** (500 MHz, DMSO-d_6, 25^{o}C): δ = 12.41 (s, 1 H, 5-OH), 10.88 (s, 1 H, 7-OH), 9.99 (s, 1 H, 3'-OH), 9.68 (s, 1 H, 3-OH), 8.21 (d, J = 7.8 Hz, 1 H, 8'-NH), 7.80 (d, J = 2.1 Hz, 1 H, 2'-H), 7.59 (dd, J = 8.6 Hz, 2.1 Hz, 1 H, 6'-H), 7.36-7.34 (m, 4 H, 15' and 16'-H), 7.30-7.26 (m, 1 H, 17'-H), 7.10 (d, J = 8.6Hz, 1 H, 5'-H), 6.44 (d, J = 2.0 Hz, 1 H, 8-H), 6.24 (d, J = 2.0 Hz, 1 H, 6-H), 4.22- 4.17 (m, 1 H, 9´-H), 3.08-2.98 (m, 2 H, 13'-H), 1.39 (s, 9 H, 12'-H) ppm; ^{13}C-NMR (500 MHz, DMSO-d_6, 25^{o}C): δ = 177.07 (C4), 171.46 (C10'), 164.95 (C7), 161.74 (C5), 157.04 (C9), 154.59 (C7'), 150.27 (C3'), 146.27 (C2), 140.87 (C4'), 138.20 (C14'), 130.03 (C15'), 129.05 (C16'), 127.32 (C17'), 124.05 (C5'), 122.45 (C1'), 119.32 (C6´), 116.59 (C2´), 104.02 (C10), 98.98 (C6), 94.14 (C8), 81.66 (C11'), 57.08 (C9'), 37.56 (C13'), 28.43 (C12') ppm. Mass characterization of **4a** and **4b** regioisomers:

Mass: MS (ESI) m/z: $[M-H]^-$ for $C_{29}H_{27}NO_{10}$: calcd: 549.16; found: 548.2.

Synthesis of 3'-O-CO-Amino acid-Quercetin (c) and 4'-O-CO-Amino acid-Quercetin (d):

To a solution of **a** and **b** (1mmol) in anhydrous dichloromethane (10 ml), TFA (1 ml) was added at 0^{o}C and the reaction was stirred at room temperature for 4 hours. After the completion of the reaction, anhydrous hexane (5 ml) was added to the reaction mixture and the yellow precipitate was filtered, washed twice with anhydrous hexane (5 ml X 2) and dried well on high vacuum to afford inseparable mixture of the regioisomers (c and d) as yellow solid.

View Article Online
DOI: 10.1039/C7OB02045G

NMR and MS characterization of 3'-O-CO-Ala-Quercetin (1c) and 4'-O-CO-Ala-Quercetin (1d) (94%).

^{1}H-NMR characterization **1c** (500 MHz, DMSO-d$_6$, 25^{o}C): δ = 12.66 (bs, 1 H, 11'-OH), 12.47 (s, 1 H, 5OH), 10.85 (s, 1 H, 7–OH), 10.39 (s, 1 H, 4'-OH), 9.56 (s, 1 H, 3-OH), 8.10 (d, J = 7.4 Hz, 1 H, 8'-NH), 7.93 (dd, J = 8.6 Hz, 2.2 Hz, 1 H, 6'-H), 7.90 (d, J = 2.2 Hz, 1 H, 2'-H), 7.09 (d, J = 8.6Hz, 1 H, 5'-H), 6.50 (d, J = 2.0 Hz, 1 H, 8-H), 6.23 (d, J = 2.0 Hz, 1 H, 6-H), 4.12- 4.09 (m, 1 H, 9′-H), 1.39- 1.37 (m, 3 H, 11′-H) ppm; ^{13}C-NMR (500 MHz, DMSO-d$_6$, 25^{o}C): δ = 176.5 (C4), 174.7 (C10'), 164.83 (C7), 161.6 (C5), 157.04 (C9), 154.46 (C7'), 152.63 (C4'), 146.57 (C2), 139.4 (C3'), 126.45 (C6′), 123.73 (C2′), 122.77 (C3), 122.66 (C1′), 117.19 (C5′), 103.95 (C10), 103.91 (C8), 99.05 (C6), 50.33 (C9'), 18.13 (C11') ppm.

^{1}H-NMR characterization **1d** (500 MHz, DMSO-d$_6$, 25^{o}C): δ = 12.66 (bs, 1 H, 11'-OH), 12.41 (s, 1 H, 5OH), 10.87 (s, 1 H, 7–OH), 9.99 (s, 1H, 3'-OH), 9.68 (s, 1H, 3-OH), 8.09 (d, J = 7.4 Hz, 1 H, 8'-NH), 7.81 (d, J= 2.1 Hz, 1 H, 2'-H), 7.61 (dd, J = 8.6 Hz, 2.2 Hz, 1 H, 6'-H), 7.19 (d, J = 8.6Hz, 1 H, 5'-H), 6.45 (d, J = 2.0 Hz, 1 H, 8-H), 6.24 (d, J = 2.0 Hz, 1 H, 6-H), 4.12- 4.06 (m, 1 H, 9′-H), 1.39- 1.37 (m, 3 H, 11′-H) ppm; ^{13}C-NMR (500 MHz, DMSO-d$_6$, 25^{o}C): δ = 176.5 (C4), 174.7 (C10'), 164.83 (C7), 161.7 (C5), 156.92 (C9), 154.46 (C7'), 150.22 (C3'), 146.39 (C2), 140.97 (C4'), 129.29 (C1′), 124.10 (C5′), 122.77 (C3), 119.23 (C6′), 116.54 (C2′), 104.06 (C10), 99.12 (C6), 94.02 (C8), 50.1 (C9'), 18.13 (C11') ppm. Mass characterization of **1c** and **1d** regioisomers:

Mass: MS (ESI) m/z: $[M+H]^+$ for $C_{19}H_{15}NO_{10}$: calcd: 417.07; found: 417.9, 438.0 $[M+Na]^+$.

NMR and MS characterization of 3'-O-CO-Leu-Quercetin (2c) and 4'-O-CO-Leu-Quercetin (2d) (90%):

^{1}H-NMR characterization **2c** (500 MHz, DMSO-d$_6$, 25^{o}C): δ = 12.67 (bs, 1 H, 10'-OH), 12.47 (s, 1 H, 5OH), 10.83 (s, 1H, 7-OH), 10.39 (s, 1 H, 4'-OH), 9.57 (s, 1 H, 3-OH), 8.07 (d, J = 8.1 Hz, 1 H, 8'-NH), 7.94 (dd, J = 8.6 Hz, 2.0 Hz, 1 H, 6'-H), 7.89 (d, J = 2.0 Hz, 1 H, 2'-H), 7.08 (d, J = 8.6Hz, 1 H, 5'-H), 6.49 (d, J = 1.8 Hz, 1 H, 8-H), 6.23 (d, J = 1.8 Hz, 1 H, 6-H), 4.08- 4.03 (m, 1 H, 9′-H), 1.82-1.76 (m, 1 H, 12'-H), 1.69-1.62 (m, 1 H, 11'a-H), 1.60-1.54 (m, 1 H, 11′b-H), 0.94 (d, J= 6.5Hz, 6 H, 13'-H) ppm; ^{13}C-NMR (500 MHz, DMSO-d$_6$, 25^{o}C): δ = 176.76 (C4), 174.77 (C10'), 164.82 (C7), 161.58 (C5), 157.95 (C9), 152.55 (C4'),

View Article Online
DOI: 10.1039/C7OB02045G

146.69 (C2), 139.7 (C3'), 136.77 (C3), 126.54 (C6'), 123.63 (C2′), 117.22 (C5′), 103.91 (C10), 99.09 (C6), 94.27 (C8), 53.08 (C9'), 40.57 (C11'), 24.95 (C12'), 22.00 (C13') ppm. ^{1}H-NMR characterization **2d** (500 MHz, DMSO-d_6, 25^{o}C): δ = 12.67 (bs, 1 H, 10'-OH), 12.41 (s, 1 H, 5OH), 10.89 (s, 1 H, 7-OH), 9.96 (s, 1 H, 3'-OH), 9.68 (s, 1 H, 3-OH), 8.07 (d, J = 8.1 Hz, 1 H, 8'-NH), 7.80 (d, J = 2.0 Hz, 1 H, 2'-H), 7.62 (dd, J = 8.6Hz, 2.0 Hz, 1 H, 6'-H), 7.18 (d, J = 8.6 Hz, 1 H, 5'-H), 6.45 (d, J = 1.8 Hz, 1 H, 8-H), 6.24 (d, J = 1.8 Hz, 1 H, 6-H), 4.08- 4.03 (m, 1 H, 9′-H), 1.82-1.76 (m, 1 H, 12'-H), 1.69-1.62 (m, 1 H, 11'a-H), 1.60-1.54 (m, 1 H, 11′b-H), 0.94 (d, J = 6.5, 6 H, 13'H) ppm; ^{13}C-NMR (500 MHz, DMSO-d_6, 25^{o}C): δ = 177.01 (C4), 174.77 (C10'), 165.09 (C7), 161.64 (C5), 157.15 (C9), 150.20 (C3'), 146.40 (C2), 141.00 (C4'), 137.76 (C3), 124.08 (C5'), 119.35 (C6′), 116.51 (C2′), 103.95 (C10), 99.24 (C6), 94.02 (C8), 53.08 (C9'), 40.57 (C11'), 24.95 (C12'), 22.00 (C13') ppm. Mass characterization of **2c** and **2d** regioisomers: **Mass:** MS (ESI) m/z: $[M+H]^{+}$ for $C_{22}H_{21}NO_{10}$: calcd: 459.12; found: 459.4.

NMR and MS characterization 3'-O-CO-Glu-Quercetin (3c) and 4'-O-CO-Glu-Quercetin (3d) (86%):

^{1}H-NMR characterization **3c** (500 MHz, DMSO-d_6, 25^{o}C): δ = 12.85 (bs), 12.47 (s, 1 H, 5-OH), 10.84 (s, 1 H, 7-OH), 10.36 (s, 1 H, 4'-OH), 9.55 (s, 1 H, 3-OH), 8.14 (d, J = 8.2 Hz, 1 H, 8'-NH), 7.92 (dd, J = 8.6 Hz, 2.2 Hz, 1 H, 6'-H), 7.79 (d, J = 2.2 Hz, 1 H, 2'-H), 7.06 (d, J = 8.6Hz, 1 H, 5'-H), 6.48 (d, J = 2.0 Hz, 1 H, 8-H), 6.23 (d, J = 2.0 Hz, 1 H, 6-H), 4.27 - 4.22 (m, 1 H, 9′H), 3.16 - 3.11 (m, 2 H, 12'-H), 3.01 - 3.29 (m, 2 H, 11'-H) ppm; ^{13}C-NMR (500 MHz, DMSO-d_6, 25^{o}C): δ = 177.01 (C4), 173.77 (C13'), 173.44 (C10'), 164.81 (C7), 161.67 (C5), 156.88 (C9), 154.99 (C7'), 152.26 (C4'), 146.70 (C2), 139.42 (C3'), 126.7 (C6′), 123.83 (C1′), 123.73 (C2'), 117.31 (C5′), 103.99 (C10), 98.98 (C6), 94.25 (C8), 56.46 (C9'), 37.36 (C11'), 37.36 (C12') ppm.

^{1}H-NMR characterization **3d** (500 MHz, DMSO-d_6, 25^{o}C): δ = 12.85 (bs), 12.41 (s, 1 H, 5-OH), 10.88 (s, 1 H, 7-OH), 9.97 (s, 1 H, 3'-OH), 9.68 (s, 1 H, 3-OH), 8.15 (d, J = 8.2 Hz, 1 H, 8'-NH), 7.78 (dd, J = 2.2 Hz, 1 H, 2'-H), 7.58 (d, J = 8.6, 2.2 Hz, 1 H, 6'-H), 7.07 (d, J = 8.4Hz, 1 H, 5'H), 6.44 (d, J = 2.0 Hz, 1 H, 8-H), 6.23 (d, J = 2.0 Hz, 1 H, 6-H), 4.27 - 4.22 (m, 1 H, 9′-H), 3.16 - 3.11 (m, 2 H, 12'-H), 3.01 - 3.29 (m, 2 H, 11'-H) ppm; ^{13}C-NMR (500 MHz, DMSO-d_6, 25^{o}C): δ = 177.01 (C4), 173.77 (C13'), 173.44 (C10'), 165.07 (C7), 161.67 (C5), 157.23 (C9), 154.99 (C7'), 150.28 (C3'), 146.50 (C2), 140.89 (C4'), 129.47 (C1′),

View Article Online
DOI: 10.1039/C7OB02045G

124.01 (C5′), 119.30 (C6'), 116.54 (C2′), 104.03 (C10), 98.98 (C6), 94.25 (C8), 56.46 (C9'), 37.36 (C11'), 37.36 (C12') ppm. Mass characterization of **3c** and **3d** regioisomers:

Mass: MS (ESI) m/z: $[M-H]^-$ for $C_{21}H_{17}NO_{12}$: calcd: 475.08; found: 474.0.

NMR and MS characterization of 3'-O-CO-Phe-Quercetin (4c) and 4'-O-CO-Phe-Quercetin (4d) (90%):

^{1}H-NMR characterization **4c** (500 MHz, DMSO-d_6, 25^{o}C): δ = 12.88 (bs, 1H, 11'-OH), 12.47 (s, 1 H, 5OH), 10.85 (s, 1H, 7-OH), 10.37 (s, 1 H, 4'-OH), 9.55 (s, 1 H, 3-OH), 8.14 (d, J = 8 Hz, 1 H, 8'-NH), 7.92 (dd, J = 8.7 Hz, 2.2 Hz, 1 H, 6'-H), 7.79 (d, J = 2.2 Hz, 1 H, 2'-H), 7.36-7.35 (m, 4 H, 14' and 15'-H), 7.31-7.26 (m, 1 H, 16'-H), 7.06 (d, J = 8.6Hz, 1 H, 5'-H), 6.48 (d, J = 2.0 Hz, 1 H, 8-H), 6.23 (d, J = 2.0 Hz, 1 H, 6-H), 4.27- 4.22 (m, 1 H, 9′-H), 3.14 (dd, J = 14.0 Hz, 4.4Hz, 1 H, 12a'-H), 2.99 (dd, J = 9.6Hz, 4.2Hz, 1 H, 12b'-H) ppm; ^{13}C-NMR (500 MHz, DMSO-d_6, 25^{o}C): δ = 174.04 (C10'), 165.03 (C7), 161.77 (C5), 157.07 (C9), 152.45 (C4'), 146.74 (C2), 139.57 (C3'), 138.64 (C13'), 130.02 (C14'), 129.01 (C15'), 127.3 (C16'), 126.70 (C6'), 123.83 (C2′), 122.63 (C1'), 117.40 (C5′), 104.00 (C10), 99.10 (C6), 94.34 (C8), 56.54 (C9'), 37.39 (C12') ppm.

^{1}H-NMR characterization **4d** (500 MHz, DMSO-d_6, 25^{o}C): δ = 12.88 (bs, 1 H, 11'-OH), 12.40 (s, 1 H, 5OH), 10.89 (s, 1 H, 7-OH), 9.97 (s, 1 H, 3'-OH), 9.67 (s, 1 H, 3-OH), 8.15 (d, J = 7.8 Hz, 1 H, 8'-NH), 7.78 (d, J = 2. Hz, 1 H, 2'-H), 7.58 (dd, J = 8.6 Hz, 2.1 Hz, 1 H, 6'-H), 7.36-7.35 (m, 4 H, 14' and 15'-H), 7.32-7.26 (m, 1 H, 16'-H), 7.07 (d, J = 8.6Hz, 1 H, 5'-H), 6.44 (d, J = 2.2 Hz, 1 H, 8-H), 6.23 (d, J = 2.2 Hz, 1 H, 6-H), 4.27- 4.22 (m, 1 H, 9′-H), 3.14 (dd, J = 14.0 Hz, 4.4Hz, 1 H, 12a'-H), 2.99 (dd, J = 9.6Hz, 4.2Hz, 1 H, 12b'-H) ppm; ^{13}C-NMR (500 MHz, DMSO-d_6, 25^{o}C): δ = 174.04 (C10'), 165.09 (C7), 161.50 (C5), 157.26 (C9), 150.15 (C3'), 146.74 (C2), 140.84 (C4'), 138.64 (C13'), 130.02 (C14'), 129.64 (C1'), 129.01 (C15'), 127.30 (C16'), 124.16 (C5'), 119.50 (C6′), 116.66 (C2′), 104.00 (C10), 99.10 (C6), 94.23 (C8), 56.54 (C9'), 37.39 (C12') ppm. Mass characterization of **4c** and **4d** regioisomers:

Mass: MS (ESI) m/z: $[M+H]^+$ for $C_{25}H_{19}NO_{10}$: calcd, 493.10; found: 516.0 $[M+Na]^+$.

Structures, molar ratios and 2D NMR spectra of the four quercetin – amino acid analogues are given in the Supplementary Information (Section 2, Supplementary Figures S2-S5).

View Article Online
DOI: 10.1039/C7OB02045G

Fluorescence spectroscopy studies

Recombinant, human protein Bcl-xL (with Δ197-233 deletions in the C-terminus and Δ45-84 internal loop between helix R1 and helix R2) was, firstly, expressed as a 6xHis-tagged protein in E. coli strain BL21 and then, purified by Ni^{2+}-affinity chromatography by Äkta Prime FPLC (GE Healthcare). Fluorescence spectroscopy studies were performed and analyzed as described in previous work[20]. Fluorescence spectra were recorded on a Perkin-Elmer LS-55 spectrofluorometer at 25 °C. Gradual concentrations of the quercetin analogues were titrated in Bcl-xL solution (2 uM) and diluted in sodium phosphate buffer (pH= 6.7). A 1.0 cm quartz cuvette was used for measurements. Bcl-xL fluorescence was collected after excitation at 285 nm. Both emission and excitation slits were set at 10 nm. The maximum emission wavelength was occurred approximately at 350 nm.

Quercetin analogues absorb at the maximum excitation and emission wavelength of Bcl-xL, due to the phenol groups that they contain. This absorption can cause quenching of the Bcl-xL fluorescence and lead to false measurements. Thus, each measurement was corrected according to the following equation [33]:

$$F_{cor} = F_{obs} 10^{-(\varepsilon_{\lambda exc} + \varepsilon_{\lambda em}) l^* L_0}$$

Where F_{obs} is the maximum measured fluorescence of Bcl-xL and F_{cor} the corrected value of the maximum fluorescence of Bcl-xL; $\varepsilon_{\lambda exc}$ or $\varepsilon_{\lambda em}$ are the molar extinction factors of Quercetin analogues at the excitation and emission wavelengths of Bcl-xL; L_0 is the total concentration of the bound and unbound Quercetin analogue; and l is the path length in the measuring cell. Data analysis achieved by hyperbola curve fitting, using Origin 8.0, according to the following equation [33, 34]:

$$F_0 - F = \frac{(F_0 - F_\infty) L_0}{K_d + L_0}$$

Where, F_0 and F are the fluorescence emission intensities in the absence and presence of the Quercetin analogue, respectively; F_∞ is a theoretically occurred value corresponding to the Bcl-xL maximum fluorescence when it is saturated; and K_d represents the binding affinity between Bcl-xL and the Quercetin analogue. Each measurement was repeated at least three times.

Isothermal Titration Calorimetry

The thermodynamic profile of the interaction between the most soluble quercetin-aminoacid conjugate, Que-Glu, and Bcl-xL was explored through isothermal titration

View Article Online
DOI: 10.1039/C7OB02045G

calorimetry. Syringe and sample cell were loaded with Que-Glu (1 mM) and Bcl-xL (0.05 mM), respectively. Recombinant human protein Bcl-xL was expressed and purified, as it is described above. Both molecules were diluted in sodium phosphate buffer containing 4% DMSO at 298 K. Each titration injected 2 μL of Que-Glu solution in the sample cell and lasted for 0.8 sec, except from the initial injection that was 0.4 μL. Overall, 17 injections were performed and the initial injection was excluded from the data analysis. A 60-sec spacing was set between the titrations. The reference power was set to 6 μcal/sec and a stirring speed equal to 1000 rpm was used for the syringe. Finally, a 3 sec filter period was applied. In order to correct the heat dilution effect, one control experiment was conducted where que-glu was titrated into the buffer and subtracted from the initial experiment. A Microcal ITC_{200} was used for the aforementioned measurements and the data were analyzed through the Origin 7.0 software provided by Microcal. The Gibbs free energy change (ΔG) was calculated using the equation $\Delta G=\Delta H-T\Delta S$.

2D NMR Spectroscopy studies

Truncated Bcl-xL was expressed and purified for NMR experiments, as we previously reported [20]. The 2D $^{1}H-^{15}N$ HSQC spectra of Bcl-xL were obtained without and with the addition of 1:1 ratio of the quercetin analogues.

Molecular Modeling

The computational workflow for the design of the new quercetin inhibitors is described in scheme 1.

View Article Online
DOI: 10.1039/C7OB02045G

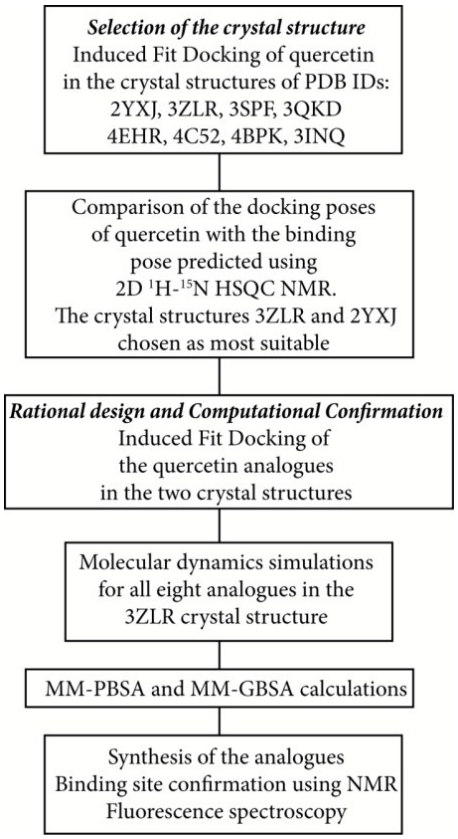

Scheme 1: Workflow for the rational design and synthesis of the quercetin analogues.

Induced Fit Docking (IFD) Simulations: The crystallographic structures of the proteins shown in Table 1 were used during the IFD simulations of quercetin. The crystal structures of the protein were prepared using the Protein Preparation Wizard[35], missing loops and side chains were prepared using Prime, ionized at a pH 7.4 using PROPKA[36], and minimized using the OPLS3 force field [37]. The structures of quercetin and its analogues were designed using Maestro 10.2, ionized at the target pH 7.4 using the Ligprep module [38], and their conformational analysis was performed using ConfGen[39]. These conformations were then submitted as starting geometries for the Induced Fit Docking calculations [40-42]. At the initial stage of docking side chains of residues that are within 5 Å of the ligand were trimmed. Three residues that are within 5 Å of the ligand and have the highest B-factors (above 40) were refined using Prime 4.0 [40]. The ligands were redocked using the extra precision mode.

Table 1: Crystallographic structures of Bcl-xL used in the IFD simulations of quercetin.

PDB Id's	Year	Resolution (Å)	Co-crystallized inhibitor
2YXJ[43]	2007	2.20	ABT-737
3ZLR[44]	2013	2.03	WEHI-539

View Article Online
DOI: 10.1039/C7OB02045G

3SPF[45]	2012	1.70	BM-501
3QKD[46]	2011	2.02	Quinazoline sulfonamide
4EHR[47]	2012	2.09	Pyrimidine phenylsulfonamide
4C52[48]	2014	2.05	Benzoylurea compound (39b)
4BPK[49]	2013	1.76	Alpha beta Puma BH3 peptide 5
3INQ[50]	2009	2.00	W1191542

Molecular Dynamics Simulations. The poses with best Induced Fit score for the eight analogues docked in the crystal structure 3ZLRwere selected as initial structures for the MD simulations. The MD simulations were carried out with the GPU version of the PMEMD module [51, 52] from the AMBER 14 simulation package [53, 54]. The geometry of every compound was optimized with the HF/6-31G* basis set (Gaussian 09) [55]. The general AMBER force field (GAFF) was used to obtain force field parameters for the compounds with RESP charges [56, 57]. The system was next solvated in a truncated octahedron with 10,170 TIP3P water molecules. The minimum distance between the edge of the periodic box and each atom of the system was set at 14 Å. The minimization of the system was carried out in four stages using restraints of 500, 10 and 2 kcal mol^{-1} $Å^{-2}$ while in the final stage no restraints were applied. During these stages, the system was minimized for 15000 steps, using a nonbonded cutoff of 20 Å. The solvated complex was then heated under constant volume for 100 ps from 0 to 310 K using a Langevin thermostat [58]. Next, the system was equilibrated under constant pressure in four stages with gradually released restraints of 100, 50, 10 and 2 kcal mol^{-1} $Å^{-2}$ for 400 ps for another 100 ps. The bonds involving hydrogen atoms were constrained at their equilibrium distance using SHAKE [59]. The collision frequency (γ) was set at 2 ps^{-1}. The simulation of each system was run for 100 ns. The analysis of the trajectories was done with the ptraj module of AMBER [60].

MM-PBSA. The molecular mechanics Poisson–Boltzmann Surface Area (MM-PBSA) method was used for the calculation of the binding energy between the eight analogues of quercetin and Bcl-xL [61-64].

10000 MD snapshots from the MD run of the complex were considered for the calculation of the enthalpy contribution (ΔH). Topology files for the complex (stripped of water), the ligands, and Bcl-xL were created using the ante-mmpbsa utility. For each snapshot, a free energy for the complex, the quercetin analogues, and Bcl-xL is calculated.

The enthalpy term is calculated as:

$\Delta H = \Delta E_{gas} + \Delta G_{solv}$, (1)

View Article Online
DOI: 10.1039/C7OB02045G

where ΔE_{gas} is defined as the molecular mechanical (MM) free energy change upon complexation of Bcl-xL with the quercetin analogues in the gas phase, while ΔG_{solv} is the solvation free energy. ΔE_{gas} is further divided into Coulomb interactions (ΔE_{ele}) and van der Waals interaction terms (ΔE_{vdW}):

$\Delta E_{gas} = \Delta E_{ele} + \Delta E_{vdW}$ (2)

The solvation term of eq. 1 is defined as a sum of polar (ΔE_{PB}) and nonpolar (ΔE_{cavity}) contributions:

$\Delta G_{solv} = \Delta G_{PB} + \Delta G_{cavity}$ (3)

Cell Culture

Two well established human prostate cell lines, DU-145 (human prostate cancer hypotriploid cell line) and PC-3 (human prostate cancer cell line) were treated with the four compounds (Que-Ala, Que-Leu, Que-Glu and Que-Phe) at concentrations ranging from 1 to 100 μM to test their cytostatic and cytotoxic activity. The cell lines were obtained from the American Type Culture Collection (ATCC) and were grown in different culture medium according to the instructions. Cells were routinely grown as monolayer cell cultures in T-75 flasks (Costar) in an atmosphere containing 5% CO_2 in air, and 100% relative humidity at 37 °C and subcultured twice a week. The culture medium used were Dulbecco's modified Eagle's medium, DMEM (Gibco, Glasgow, UK) (for DU-145 cell line) and RPMI 1640 medium (for PC-3 cell line) (Roswell Park Memorial Institute medium) (Gibco, Glasgow, UK), both supplemented with 10% fetal bovine serum (Gibco, Glasgow, UK), 2 mM glutamine (Sigma), 100 μg/mL streptomycin and 100 IU/mL penicillin. Adherent cells at a logarithmic growth phase were detached by addition of 2–3 mL of a 0.05% trypsin (Gibco) – 0.02% EDTA mixture and incubation for 2–5 min at 37 ˚C. The loss of membrane integrity, as a morphological characteristic for cell death, was assayed by Trypan Blue exclusion. All chemicals and solvents used were of high purity and purchased from Sigma or Merck.

MTT assay

The MTT ((3-(4, 5-imethylthiazol-2-yl)-2, 5-diphenyltetrazolium bromide) assay is a well-established and standard method for evaluating the cytostatic and cytotoxic activity of drugs and chemicals. Briefly, the cells were plated in 96-well flat-bottom microplates (Costar-Corning, Cambridge) (100 μL containing 5,000 cells/well for PC-3 and 8,000 cells/well for

View Article Online
DOI: 10.1039/C7OB02045G

the rest cell lines) and maintained for 72 h at 37 °C in a 5% CO_2 incubator and grown as monolayers. After 24 h, cells were treated with 1–100 μmol/l of the compounds for 48 h. The viability of cultured cells was estimated using MTT (Sigma, St Louis, Missouri, USA) metabolic assay as described previously. MTT was dissolved in PBS in a concentration of 5 mg/mL, filter sterilized, and stored at 4°C. MTT (50 μL of stock solution) was added to each culture and incubated for 3 h at 37 °C to allow metabolization. Formazan crystals were solubilized by DMSO (100 μL) Absorbance of the converted dye was measured at a wavelength of 540 nm on an ELISA reader (Versamax, Orleans, USA)[65].

The mean concentrations of each drug that generated 50% or total (100%) growth inhibition (GI50 and TGI, respectively) as well as the drug concentrations that produced cytotoxicity against 50% of the cultured cells [(half maximal cytotoxic concentration (IC50)] were calculated using the linear regression method. GI50 and TGI concentrations calculated after 48 h exposure. Results are mean of three independent experiments. GI50 was calculated as the drug concentration that reduced the number of cells to 50% of the number of cells before each compound addition. TGI is the drug concentration that achieved total growth inhibition of the cells. Using seven absorbance measurements [time 24 h (Ct24), control growth 72 h (Ct72), and test growth in the presence of drug at five concentration levels (Tt72x)], the percentage of growth was calculated at each level of the drug concentrations. The percentage growth inhibition was calculated according to National Cancer Institute (NCI) as: [(Tt72x) - (Ct24)/(Ct72) - (Ct24)] × 100 for concentrations for which Tt72x>Ct24 and [(Tt72x) - (Ct24)/Ct24] × 100 for concentrations for which Tt72x< Ct24; GI50 was calculated from [(Tt72x)-(Ct24)/(Ct72) - (Ct24)] × 100 = 50,TGI from [(Tt72x) - (Ct24)/(Ct72) - (Ct24)] × 100 = 0, and IC_{50} from [(Tt72x) - (Ct24)/Ct24] × 100 = 50. All the experiments were carried out in triplicate.

Results and Discussion

Computational Approaches

IFD simulations and rational design: To rationally design the quercetin-amino acid analogues able to bind to the BH3 binding site of Bcl-xL we used for the IFD process the different available crystal structures shown in Table 1. Since the preferred binding site of quercetin for Bcl-xL has already been described by Tzakos *et al.*[20] this information was used to validate the docking poses of quercetin in the eight different crystal structures. Although all eight crystal structures predicted the binding site for quercetin[20] only the structures with

View Article Online
DOI: 10.1039/C7OB02045G

PDB ID 3ZLR [44] and 2YXJ [43] provided the binding poses with the highest GlideScore and the best correlation with our previously published 2D ^{1}H-^{15}N HSQC NMR data[20]. As can be observed in Figure 2A quercetin is inserted in the hydrophobic pocket P2 with its B ring directed towards the surface of the protein. Although quercetin develops multiple interactions with Bcl-xL it cannot interact with polar residues such as Tyr195, Arg139, Tyr101 (Figure 2C) that are located in the neighborhood of ring B and play an important role in the binding of ABT737 and WEHI-539 [43, 44]. Addition of a complementary negatively charged group to the ring B of quercetin and specifically at positions 3′ or 4′ could develop favorable interactions with the neighborhood positively charged residues of Bcl-xL such as Arg139 and Asn136 (Figure 2B). To achieve this we envisaged conjugating different amino acids at the 3′ or 4′ positions of quercetin via their α-amino group through carbamate bonds (Figure 2D). To evaluate this, substitutions at both positions were investigated computationally. Quercetin was conjugated with 4 representative residues: alanine (the simplest residue after glycine), leucine (hydrophobic), phenylalanine (aromatic) and glutamic acid (negatively charged). All eight generated compounds have a negatively charged carboxyl group that can opperate as a hydrogen bond acceptor for the positively charged residues of the surface of Bcl-xL.

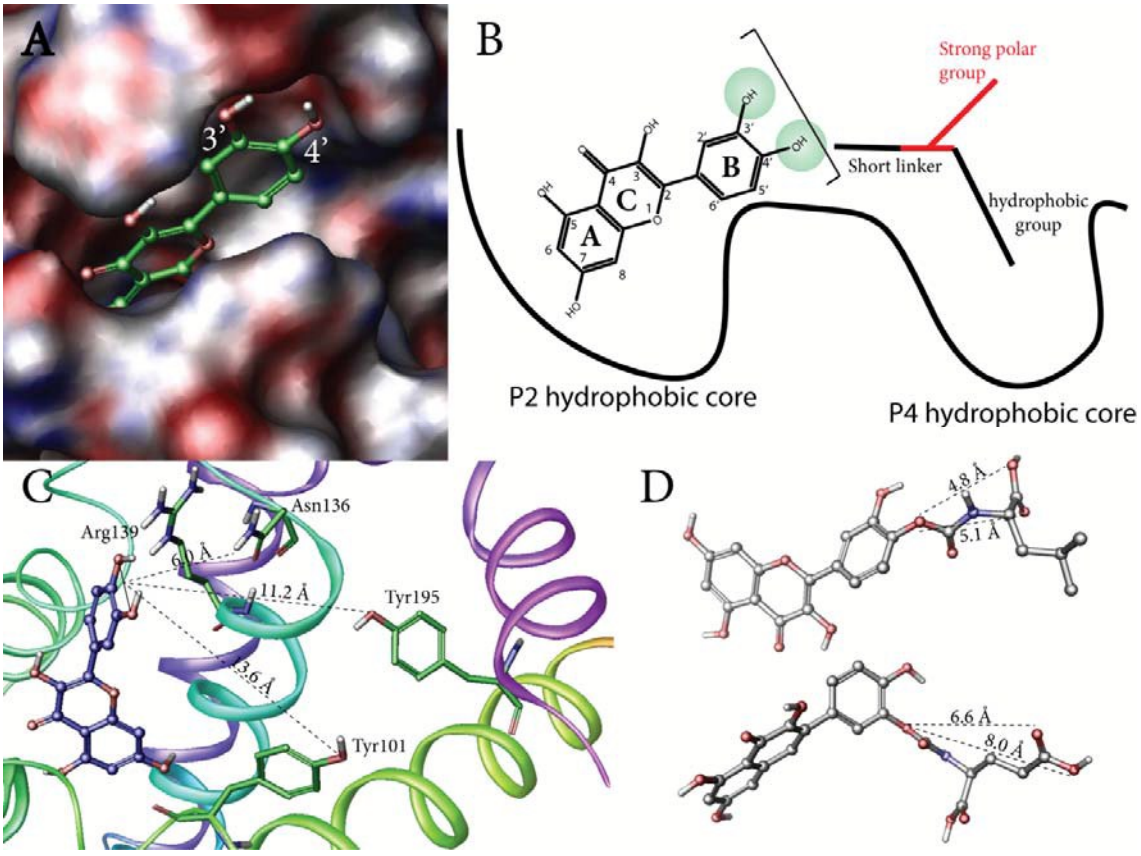

View Article Online
DOI: 10.1039/C7OB02045G

Figure 2: (A) Binding pose of quercetin[44]. (B) Rational design of quercetin analogues. (C) The average distance from the 4′ and 3′ positions and the polar residues Asn136, Tyr195 and Tyr101. (D) Quercetin substituted at the 4′ position with the residue leucine (top) and at the 3′ position by glutamic acid (bottom). The exposed carboxyl group is situated at a distance of 5 Å from the positions 3′ and 4′, in order to develop hydrogen bonds with Asn136. This suggests the linking of the amino acids via carbamate bonds. The second carboxyl group in the case of quercetin –glutamic acid conjugate is located in the appropriate position to develop interactions with the polar residues Tyr195 and Tyr101.

Figure 3 illustrates the binding poses of the quercetin analogues substituted at the 3′ position (defined through the text as Que-amino acid3). The carboxyl group of Que-Ala3 develops multiple hydrogen bonds with Arg139 and Asn136. The hydroxyl groups at positions 3 and 5 develop hydrogen bonds with Ser106 and Leu108. Glu98 develops a hydrogen bond with the hydroxyl group at position 7 of quercetin segment (Figure 3A). Multiple hydrophobic interactions are also developed with quercetin segment and Bcl-xL residues Ala142, Phe146, Ala149, Phe97, Trp137 and Tyr101 (Figure S14A). The two carboxyl groups of the Que-Glu3 analogue develop hydrogen bonds with residues Arg139, Asn136, Tyr101 and Tyr195. Hydrogen bonds are also developed between the hydroxyl group at position 5 of the compound and Leu108 and Ser106 (Figure 3B and Figure S14B). Identical hydrogen bonds are also developed by Que-Phe3. Furthermore, the development of π-π stacking interactions of quercetin segment with Phe105 and Tyr195 (Figure 3C and S14C) were observed. The analogue Que-Leu3 develops multiple hydrogen bonds with residues Asn136, Arg139, Asp133, Ala142 and Ser106 (Figure 3D and S14D). The binding poses of these compounds in the crystal structure 2YXJ illustrate very similar interactions (Figure S16 and S17). The Que-Ala3 analogue develops multiple hydrogen bonds with Ala142, Leu130, Arg139 and Asn136 (Figure S16A and S17A). The rest of the analogues develop the same described interactions and additionally a hydrogen bond with Tyr101 (Figure S16 and S17).

View Article Online
DOI: 10.1039/C7OB02045G

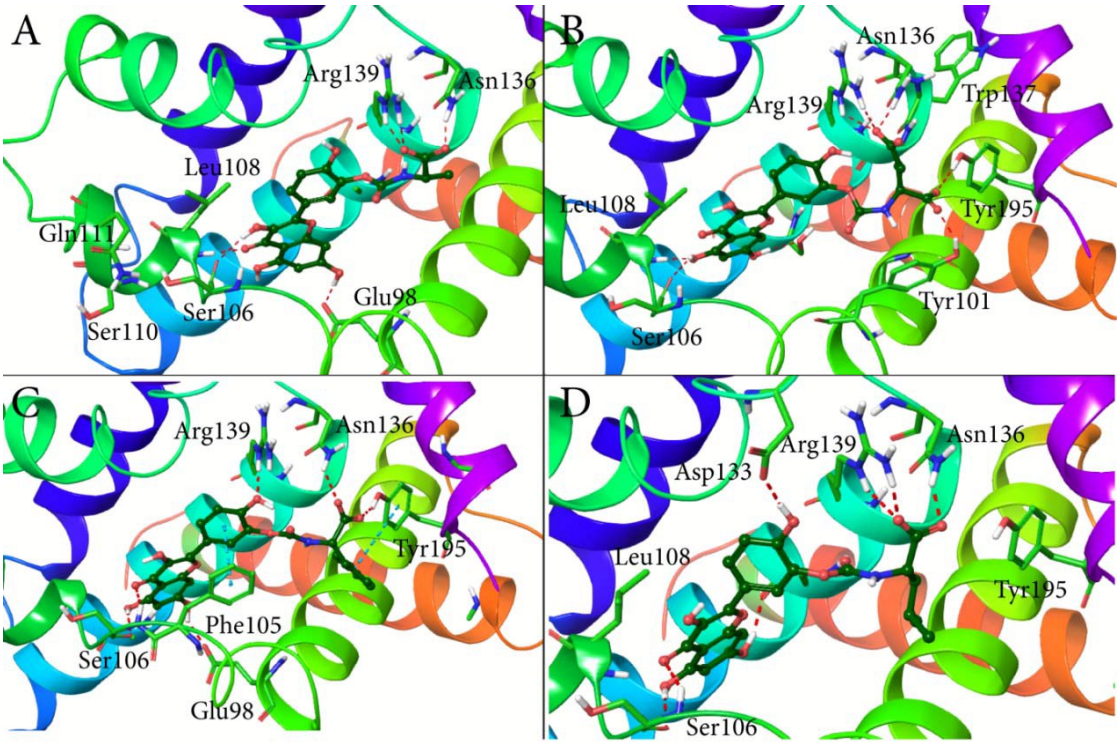

Figure 3: Binding poses of the quercetin analogues: A) Que-Ala3; B) Que-Glu3; C) Que-Phe3 and D) Que-Leu3 in the crystal structure of Bcl-xL with PDB ID 3ZLR.

The binding poses of the quercetin analogues substituted at 4′ (defined through the text as Que-amino acid4) are illustrated in Figure 4. The critical residues that develop interactions remain mostly the same. Que-Ala4 develops hydrogen bonds with Ser106, Leu108, Arg139, Asn136, Tyr101 and Glu98 (Figure 4A and S15A). The residues Ser106, Ser145, Asn136, Arg139, Tyr195, Gly138 develop hydrogen bonds with Que-Glu4. Furthermore, a π-π stacking interaction is developed with Phe105 (Figure 4B and S15B). Similar interactions are developed between the other two analogues (Que-Phe4 and Que-Leu4) and Bcl-xL (Figure 4C, D and S15C, D). Similar binding poses are predicted by the IFD calculations of the four compounds in the 2YXJ crystal structure (Figures S18 and S19).

To better evaluate the binding poses of the newly designed compounds they were superimposed with the crystal structures of the established Bcl-xL inhibitors ABT-737 and WEHI-539 (in Figure 5 is shown the Que-Glu3 analogue). As it can be observed in Figure 5A both ABT-737 and the newly synthetic conjugate bind in the same manner to the Bcl-xL protein. The rings A, B and C of the Que-Glu3 analogue bind to the hydrophobic core P2 as does the 2-(4-chlorophenyl)phenyl]methyl moiety of ABT-737 (Figure 5A,B) and the 1,3-benzothiazol-2-ylhydrazinylidene moiety of WEHI-539 (Figure 5 C,D). The carboxyl part of

View Article Online
DOI: 10.1039/C7OB02045G

Que-Glu3 analogue overlaps with the sulfonyl moiety of ABT-737 (red circle in Figure 5B) and the carboxyl moiety of WEHI-539 (red circle in Figure 5D). These superimpositions suggest that the designed quercetin analogues possess the appropriate hydrophobic moiety to interact with the P2 core and the negatively charged moieties to interact with the positively charged residues located in the protein surface.

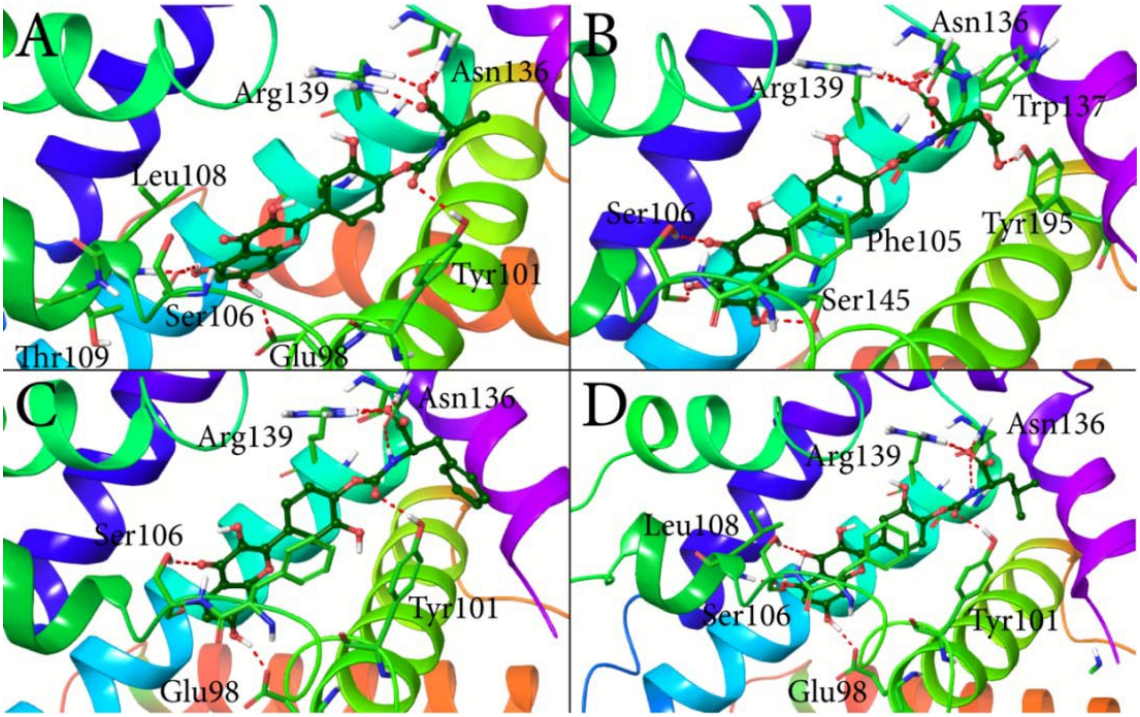

Figure 4: Binding poses of the quercetin analogues: A) Que-Ala4; B) Que-Glu4; C) Que-Phe4 and D) Que-Leu4 in the crystal structure of Bcl-xL with PDB ID 3ZLR.

View Article Online
DOI: 10.1039/C7OB02045G

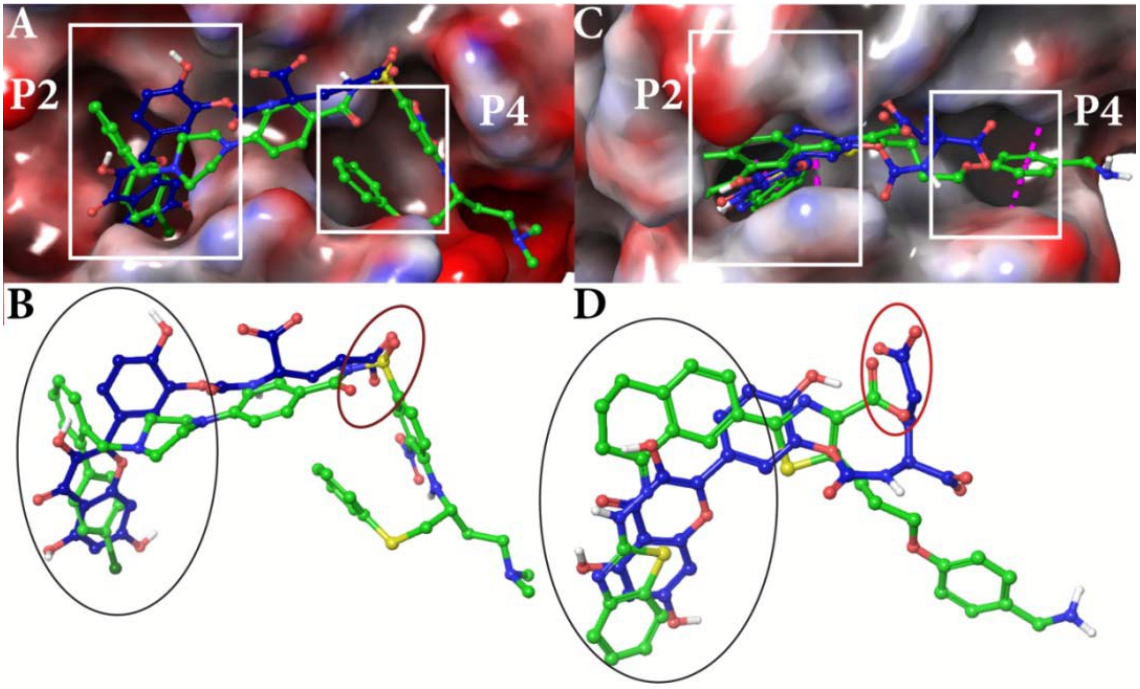

Figure 5: A, B) Superimposition of the Que-Glu3 analogue (carbon atoms are in blue color) to the ABT-737 structure (carbon atoms are in green color). C, D) Superimposition of the Que-Glu3 analogue to the WEHI-539. In panels A and C the surface of the protein is showed using an electrostatic potential map (red negative, blue positive, white neutral).

Molecular Dynamics Simulations: To assess the stability of the quercetin-analogues – Bcl-xL complexes MD simulations of 100 ns were run for all analogues using the coordinates of Bcl-xL from the PDB ID 3ZLR [44]. The root mean squared deviations (RMSDs) of the protein and ligands are shown in Figure 6. As previously reported by Guo *et al.* [66] the RMSDs of the complexes reach a stable equilibrium after 20 ns in most cases. The average RMSD for the simulations goes from 5 Å (in the case of Que-Glu4) to 12 Å for Que-Leu3. These numbers are larger compared to other simulations reported by Novak *et al.* [67] probably due to the shorter simulation time in the latter case. The lower RMSDs of the protein in its bound states manifest a ligand stabilization effect on the flexible region of the active site [66]. As a result the analogues Que-Glu3, Que-Glu4 and Que-Phe4 that display the lowest RMSDs display the largest ligand stabilization effects.

The root mean squared fluctuations (RMSF) of the Cα atoms of all eight simulation systems over the MD runs are shown in Figure 6. The more flexible regions are highlighted by higher RMSF values. The connecting loop between α1 and α2 helices (residues 29-42) is the most flexible region as previously reported by Guo *et al.*[66]. The loop residues fluctuate at an average RMSF of around 5Å. The disordered nature of this segment can explain these high

View Article Online
DOI: 10.1039/C7OB02045G

fluctuations. The residues around the binding pocket (95-150) show an average RMSF of 1-2 Å and do not display the significant deviations of an average RMSF of 4 Å reported by Guo *et al*. [66] signifying the further stabilization of the newly synthesized analogs to the highly flexible BH3 binding site.

Hydrogen bond analyses of all trajectories are shown in Table 2. The analogue Que-Ala3 develops multiple H-bond interactions with the residues Arg103, Asn136 and Arg139. These interactions are very stable over time. Two further interactions are developed with Ala104 and Ser106. Que-Ala4 does not develop interactions with the residues Arg103, Ala104 and Asn136 but present a very stable H-bond with Ser106 (94% of the simulation time). Furthermore, interactions are developed with residues Thr109, Arg132 and Ser145. The Que-Glu3 analogue develops multiple interactions with the residues Arg100, Tyr101, Asn136, and Arg139. A stable H-bond (75.54% of the simulation time) is developed with Ser106. The Que-Glu4 analogue develops multiple H-bonds with Tyr101, Arg139 and Ser145. Stable H-bonds are also developed with Glu98, Ser106, Thr109, Arg132 and Asn136. The Que-Phe3 and Que-Phe4 analogues develop few H-bonds mainly with Ser106, Asn136 and Arg139. The same interactions are developed for the Que-Leu analogues. From these analyses it became evident that the hydrogen bonds developed among the quercetin analogues and the positive patch (localized in the neighborhood of ring B of quercetin and consisted of the polar residues Asn136 and Arg139), are stable (> 50% of the simulation time) for all analogues. This evidence aligns with our initial hypothesis that incorporating a negative charge close to ring B of quercetin could lead to analogues developing favorable interactions with the positively charged patch localized in the neighborhood of the Bcl-xL protein surface.

View Article Online
DOI: 10.1039/C7OB02045G

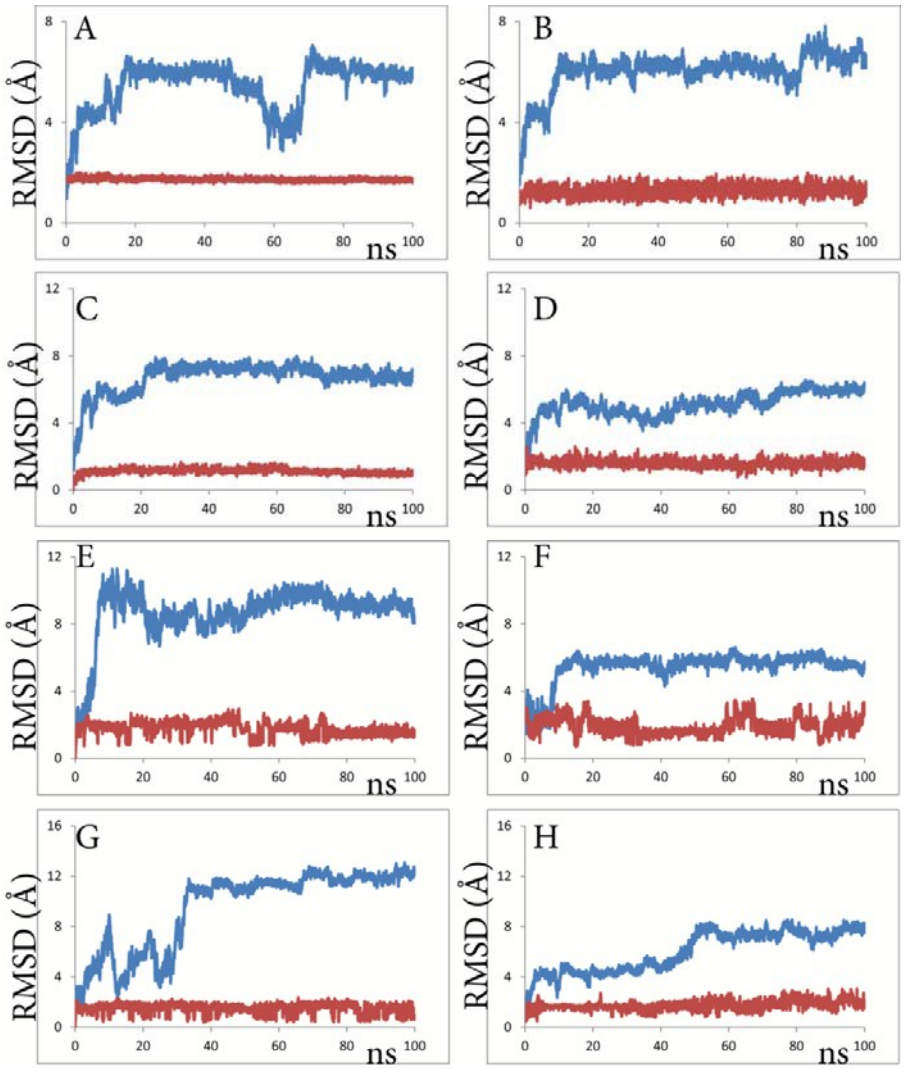

Figure 6: RMSD of the backbone of the protein Bcl-xL (in blue) and the ligands (in red): A) Que-Ala3; B) Que-Ala4; C) Que-Glu3; D) Que-Glu4; E) Que-Phe3; F) Que-Phe4; G) Que-Leu3 and H) Que-Leu4.

View Article Online
DOI: 10.1039/C7OB02045G

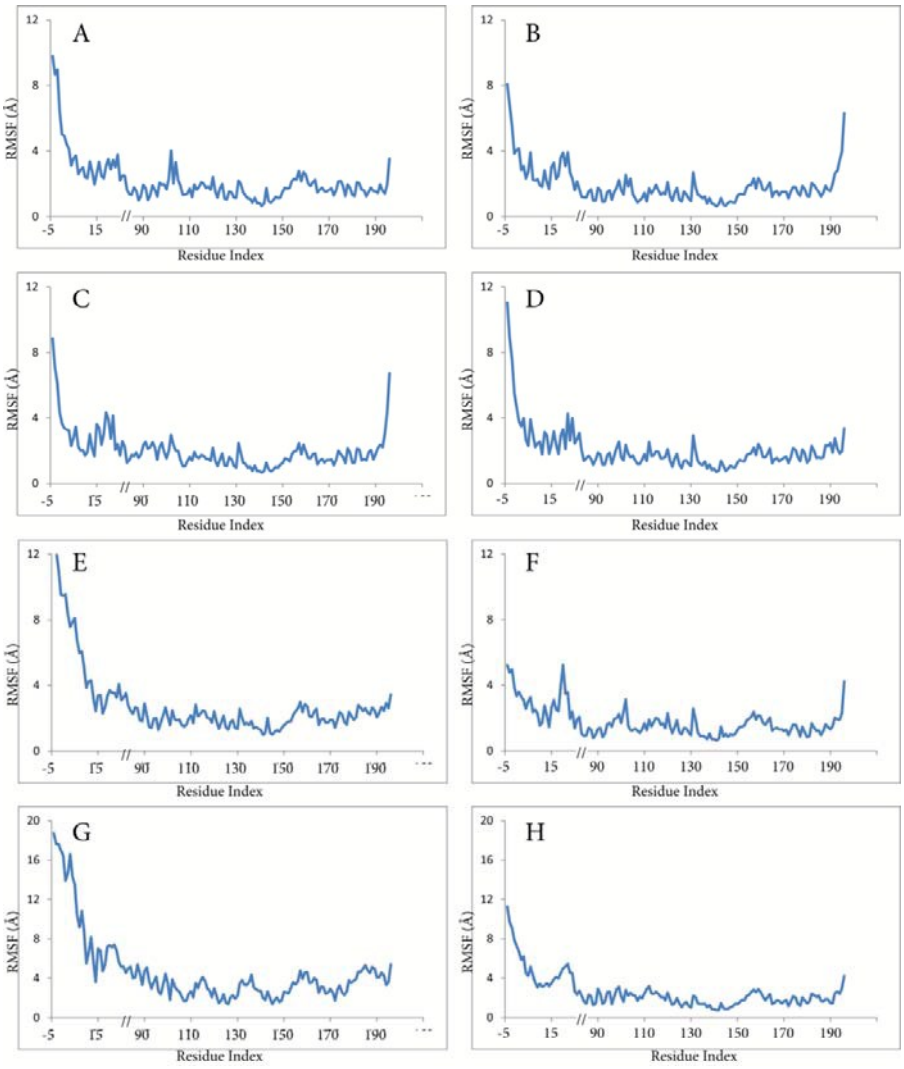

Figure 7: RMSF of the protein's residues in the Cα atoms for the analogues A) Que-Ala3; B) Que-Ala4; C) Que-Glu3; D) Que-Glu4; E) Que-Phe3; F) Que-Phe4; G) Que-Leu3 and H) Que-Leu4.

View Article Online
DOI: 10.1039/C7OB02045G

Table 2: Occurrence of hydrogen bonds between the quercetin analogues and the Bcl-xL protein.

	Occurrence [a]							
Residues in H-bonds	**Que-Ala3**	**Que-Ala4**	**Que-Glu3**	**Que-Glu4**	**Que-Phe3**	**Que-Phe4**	**Que-Leu3**	**Que-Leu4**
Glu98				27.00				
Arg100			67.89/59.07 /57.40/34.94					
Tyr101			66.39/24.46 /19.63	34.38/10.50				
Arg102							24.12	
Arg103	44.50/17.37 /15.87/14.88 [b]							
Ala104	12.75							
Ser106	10.37	94.00	75.54	82.50	88.00	27.00	77.00	41.43
Thr109		22.88		13.25				
Arg132		48.88		15.13				
Asn136	42.88/38.37		50.29/44.76	11.25	32.88/25.00	34.75/18.87	25.25/23.25	25.46/23.96
Arg139	49.25/41.50 /14.88/12.00	70.63/69.00 /46.13/38.00	57.40/52.5 /43.59/38.27	68.88/62.50 /52.88/37.87	40.38/33.75 /28.12/26.37	36.50/31.00 /26.12/16.50	44.25/39.88 /32.88/27.88	46.09/45.09 /43.76/41.26
Ser145		89.88		65.50/13.00			20.87/17.25	

[a]Occurrence is defined as the percentage of simulation time that a specific interaction exists; interactions occurring less than 10% of the simulation are not shown. [b] Multiple hydrogen bonds are formed between different atoms of the inhibitor and the specific residue.

MM-PBSA and MM-GBSA calculations: To assess the theoretical binding affinities of all complexes MM-PBSA and MM-GBSA calculations were run on all eight simulation trajectories to measure the binding enthalpies for all eight compounds. The average values for all analogues are shown in Tables 3 and 4. The MM-PBSA calculations pinpoint that the Que-Glu3 analogue displays the highest binding enthalpy (-47.16 kcal/mol). The change from Que-Glu3 to Que-Glu4 causes a higher enthalpy with a difference of 16 kcal/mol ($\Delta H_{Que\text{-}Glu4}$ = -31.05 kcal/mol). The most favored enthalpies after the Que-Glu3 analogue are displayed by the Que-Ala3 analogue (-36.65 kcal/mol) and the Que-Phe4 analogue (-36.48 kcal/mol).

View Article Online
DOI: 10.1039/C7OB02045G

All other analogues display similar enthalpies that averages from -27.33 kcal/mol (Que-Leu3) to -33.82 (Que-Leu4). Per-residue free energy decomposition (Table S2) revealed that the energy contributions of Arg139, Asn136, Phe146, Leu130, Ala142, Ser106, Phe105 Asp107, Leu108, Phe97 play a major role in determining the MM-PBSA score. The MM-GBSA scores shown in Table 4 further corroborate the indication that the Que-Glu3 analogue could present the most favored binding profile among all eight analogues. The other seven analogues display similar enthalpies between them making it difficult to decide their ranking.

Table 3: Binding enthalpies for the analogues of quercetin, as calculated using the MM-PBSA utility.

	Average value (kcal/mol) [±SEM[1]]							
Energy Component	Que-Ala3	Que-Ala4	Que-Glu3	Que-Glu4	Que-Phe3	Que-Phe4	Que-Leu3	Que-Leu4
ΔE_{vdw}	-52.67 [0.43]	-43.63 [0.04]	-51.89 [0.39]	-41.08 [0.05]	-54.37 [0.07]	-43.80 [0.35]	-49.45 [0.07]	-41.76 [0.38]
ΔE_{elec}	-24.69 [1.99]	21.05 [0.25]	89.15 [2.31]	98.47 [0.35]	39.07 [0.33]	33.96 [1.85]	25.63 [0.26]	31.57 [2.11]
ΔG_{PB}	45.04 [1.75]	-2.88 [0.20]	-79.94 [1.83]	-84.34 [0.33]	-11.18 [0.25]	-21.90 [1.54]	0.97 [0.24]	-19.19 [1.87]
ΔG_{cavity}	-4.34 [0.02]	-3.90 [0.00]	-4.50 [0.02]	-4.10 [0.00]	-4.90 [0.00]	-4.19 [0.02]	-4.48 [0.00]	-4.38 [0.02]
ΔE_{gas}	-77.35 [2.1]	-22.58 [0.24]	37.27 [2.19]	57.39 [0.35]	-15.30 [0.31]	-10.31 [1.88]	-23.81 [0.26]	-10.24 [2.12]
ΔG_{solv}	40.70 [1.74]	-6.78 [0.20]	-84.45 [1.83]	-88.44 [0.33]	-16.08 [0.26]	-26.16 [1.54]	-3.51 [0.24]	-23.57 [1.86]
$\Delta H=\Delta E_{gas}+\Delta G_{solv}$	**-36.65 [0.89]**	**-29.36 [0.07]**	**-47.16 [0.88]**	**-31.05 [0.09]**	**-31.39 [0.10]**	**-36.48 [0.87]**	**-27.33 [0.08]**	**-33.82 [0.85]**

[1]Standard error of the mean (SEM): SEM = Standard deviation/√N. N is the number of trajectory frames used during the MM-PBSA calculations

Table 4: Binding enthalpies for the analogues of quercetin, as calculated using the MM-GBSA utility.

View Article Online
DOI: 10.1039/C7OB02045G

	Average value (kcal/mol) [±SEM[1]]							
Energy Component	Que-Ala3	Que-Ala4	Que-Glu3	Que-Glu4	Que-Phe3	Que-Phe4	Que-Leu3	Que-Leu4
ΔE_{vdw}	-41.79 [0.07]	-43.63 [0.04]	-51.91 [0.06]	-41.08 [0.05]	-54.37 [0.07]	-43.79 [0.06]	-49.45 [0.07]	-41.79 [0.07]
ΔE_{elec}	30.75 [0.24]	21.05 [0.25]	89.12 [0.38]	98.47 [0.35]	39.07 [0.33]	33.50 [0.22]	25.63 [0.26]	30.75 [0.24]
ΔG_{GB}	-20.38 [0.21]	-8.99 [0.21]	-82.75 [0.36]	-86.57 [0.33]	-15.90 [0.26]	-22.40 [0.19]	-7.59 [0.24]	-20.38 [0.21]
ΔG_{cavity}	-5.960 [0.00]	-5.76 [0.00]	-6.94 [0.00]	-5.99 [0.00]	-6.99 [0.00]	-5.42 [0.00]	-6.41 [0.00]	-5.96 [0.00]
ΔE_{gas}	-11.03 [0.23]	-22.57 [0.24]	37.21 [0.38]	57.39 [0.35]	-15.30 [0.31]	-10.28 [0.21]	-23.81 [0.26]	-11.03 [0.23]
ΔG_{solv}	-26.34 [0.21]	-14.76 [0.21]	-89.69 [0.36]	-92.56 [0.32]	-22.89 [0.26]	-27.83 [0.19]	-14.00 [0.23]	-26.34 [0.21]
$\Delta H=\Delta E_{gas}+\Delta G_{solv}$	**-37.38 [0.06]**	**-37.34 [0.06]**	**-52.47 [0.08]**	**-35.16 [0.07]**	**-38.20 [0.06]**	**-38.11 [0.07]**	**-37.82 [0.07]**	**-37.38 [0.06]**

[1]Standard error of the mean (SEM): SEM = Standard deviation/√N. N is the number of trajectory frames used during the MM-PBSA calculations

Synthesis of the quercetin – amino acid conjugates

Based on the *in silico* findings we then proceeded to the synthesis of four quercetin – amino acid conjugates with glutamic acid, alanine, phenylalanine and leucine. The conjugates were made by direct coupling of the α-amine of the amino acids to the phenol groups located in ring B of quercetin through a carbamate bond. On the frame of this synthetic scheme the coupling of the α -carboxylic group of the coupled amino acids is left exposed for developing interactions with the protein. For the synthesis we used the previously published scheme[30] with some modifications (See Material and Methods) that enabled us to enhance the yield of the coupling reaction and therefore the overall yield by 10-15%. Following this reaction scheme we obtained for all the conjugates two inseparable regioisomers at approximately 3:1. Triggered by the *in silico* data indicating that both regioisomers presented similar interaction profile and binding poses, the regioisomers were used for *in vitro* evaluation.

Validation of the quercetin – amino acid conjugates binding to Bcl-xL

View Article Online
DOI: 10.1039/C7OB02045G

To evaluate the binding of the different quercetin analogues to Bcl-xL we conducted steady state fluorescence spectroscopy experiments. The basis of this technique lies upon the alterations that occur on the tryptophan fluorescence intensity, when a ligand binds to the protein. Here, the addition of incremental concentrations of quercetin-alanine, quercetin-leucine, quercetin-glutamic acid and quercetin-phenylalanine caused quenching of the intrinsic tryptophan fluorescence (Table 5 and Supplementary Fig. S20-S23). Through this study we determined that all analogues bind to Bcl-xL. The binding affinities of the interactions were calculated with no considerable differences existing among them. However, this happens, mainly, due to the low sensitivity of the technique, since tryptophan's fluorescence intensity is low and we cannot export further clear conclusions about which interaction is the strongest. To further evaluate the thermodynamics of the interaction we utilized a more sensitive technique that is Isothermal Titration Calorimetry (ITC). ITC monitors the heat that is created or absorbed during an interaction, and thus can calculate the changes in enthalpy (ΔH), entropy (ΔS) and Gibbs free energy (ΔG), as well as the association constant (K_a). From the four synthesized analogues we were able to record only the interaction between Que-Glu and Bcl-xL (Figure 8) since ITC requires the dilution of protein and ligand in the same solvent, that due to Bcl-xL is limited to water. The aqueous solubility of the hybrids has been formerly been determined by Kim et al. and Que-Glu was determined the one to present the highest hydrophilicity (up to 53-fold) with respect to the parent compound[30]. Moreover, we utilized RP-HPLC, which is a widely used technique to calculate the relevant hydrophilicity of the analogues based on the retention times[68]. Based on these results (Retention times can be found in Supplementary data Table S3) it became evident that the only analogue that could conform to the required ITC conditions was Que-Glu and was used for ITC.

Table 5: Binding affinities of Bcl-xL interaction with the Quercetin analogues

Compound	K_d (μM)	Standard Error
Que-Glu	2.8	0.1
Que-Leu	8.2	0.1
Que-Phe	5.3	0.2
Que-Ala	8.7	0.2

The thermodynamic parameters of the Que-Glu Bcl-xL as derived from ITC are illustrated in Table 6. The interaction is exothermic and spontaneous as the negative changes

View Article Online
DOI: 10.1039/C7OB02045G

in enthalpy and Gibbs free energy indicate. The determined value of the association constant (Ka) showed a modest affinity (Kd = 22 μM) of Que-glu to Bcl-xL. Finally, the negative and positive change in enthalpy (ΔH<0) and entropy (ΔS>0) respectively, point out that both hydrogen bonding and hydrophobic interactions participate in the binding process.

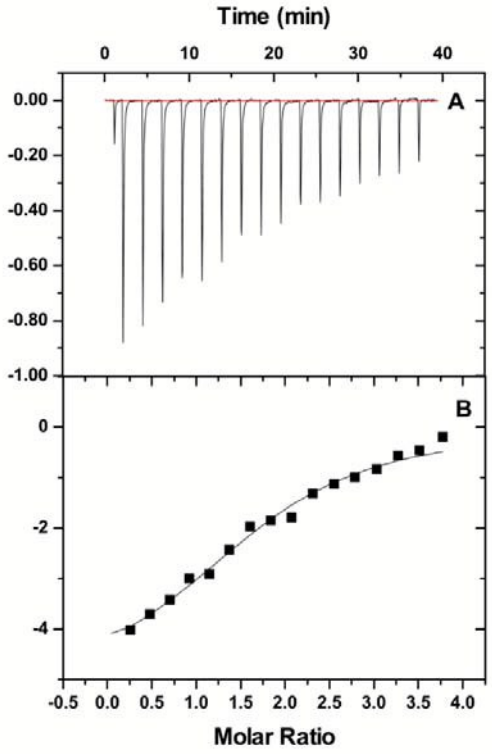

Figure 8. Isothermal Titration calorimetry experiment between Que-Glu (1 mM) and Bcl-xL (0.05 mM) at 298 K: A) Isothermal curves, B) Fitted sigmoidal curve (the first injection was excluded)

Table 6. Thermodynamic parameters of the Bcl-xL – Que-Glu interaction

K_a (M^{-1})	ΔH (kcal/mol)	-TΔS (kcal/mol)	ΔG (kcal/mol)	N
45100 ±9290	-5.2 ±0.4	-1.1	-6.3	1.69

Charting the binding site of the different quercetin-amino acid conjugates to the Bcl-xL interface

To map the ligand-protein binding interface, we monitored the binding of the four quercetin analogues (Que-Ala, Que-Phe, Que-Leu, and Que-Glu) to Bcl-xL by using chemical shift perturbation mapping through NMR. Fig. 8 illustrates the overlaid 2D ^{1}H-^{15}N HSQC spectra

View Article Online
DOI: 10.1039/C7OB02045G

of Bcl-xL in the absence or presence of the quercetin analogues. We found that significant line-broadening and chemical shift changes of numerous ^{1}H-^{15}N crosspeaks in Bcl-xL occurred upon the addition of the quercetin analogues, indicating the direct interaction of Bcl-xL with them (Supplementary Fig. S24). Furthermore, the NMR chemical shift perturbations induced by binding to the quercetin analogues were localized to the hydrophobic BH3 binding groove surrounded by the BH1, BH2 and BH3 domains of Bcl-xL, which are in good agreement with those previously observed during the binding of Quercetin to Bcl-xL and BCL-2 [20]. Weighted ΔCS values were calculated using the equation $\Delta CS = [(\Delta^{1}H)^{2} + 0.2(\Delta^{15}N)^{2}]^{0.5}$ and are depicted in Figure 10 and Supplementary Table S1. The disappearance of such crosspeaks arises from intermediate chemical exchange at the NMR time scale, indicating that the missing residues are involved in ligand binding. As can be seen in Figure 10 the peaks of the residues Ala104 and Ser106 disappear completely after the addition of the compounds. This is in agreement with the modeling data since most compounds develop hydrogen bonds with these two residues (in particular the hydroxyl groups at positions 5 and 7 [Figures S14 and S15]). The residues S110, Q111, and W137 might be involved in the binding-induced structural change because they are located in the flexible loop. The peaks of Glu98, Ala142 and Arg139, in the cases of the compounds Que-Glu, Que-Phe and Que-Leu disappear completely. This conforms to the binding poses of these compounds since most of them develop hydrogen bonds with these residues (Figures 3 and 4). The peak of the residue Ser145 also disappears when the compounds Que-Ala, Que-Phe and Que-Leu are added, while in the case of the Que-Glu compound it shows a ΔCS of 0.089 (Supplementary Table S1). This residue forms a hydrogen bond with the hydroxyl group at position 7 in the case of Que-Ala4 (Supplementary Figure S19) while in all other cases it is very close (< 4 Å) to the quercetin moiety of the compounds. The peaks of the residues Tyr101 and Tyr195 also disappear in the cases of the addition of the compounds Que-Glu, Que-Phe and Que-Leu. IFD poses in Figs. 3 and 4 show that the residues form hydrogen bonds with the carboxyl group or π-π stacking with the phenyl group in the case of Que-Phe. The chemical shift of Asn136 is 0.24 in the case of Que-Phe and 0.09 in the cases of Que-Glu and Que-Leu (Supplementary Table 1) showing that the polar residue is involved in the binding as initially designed and predicted by both MD simulations and IFD poses. The involvement of Asn136 in the binding could explain the ΔCS changes in the cases of the neighboring residues such as Trp137. Residues such as Leu130 and Ile140 although in most cases are not involved in hydrogen bonding, develop hydrophobic interactions with the compounds and are in the vicinity of the binding site of the ligands.

View Article Online
DOI: 10.1039/C7OB02045G

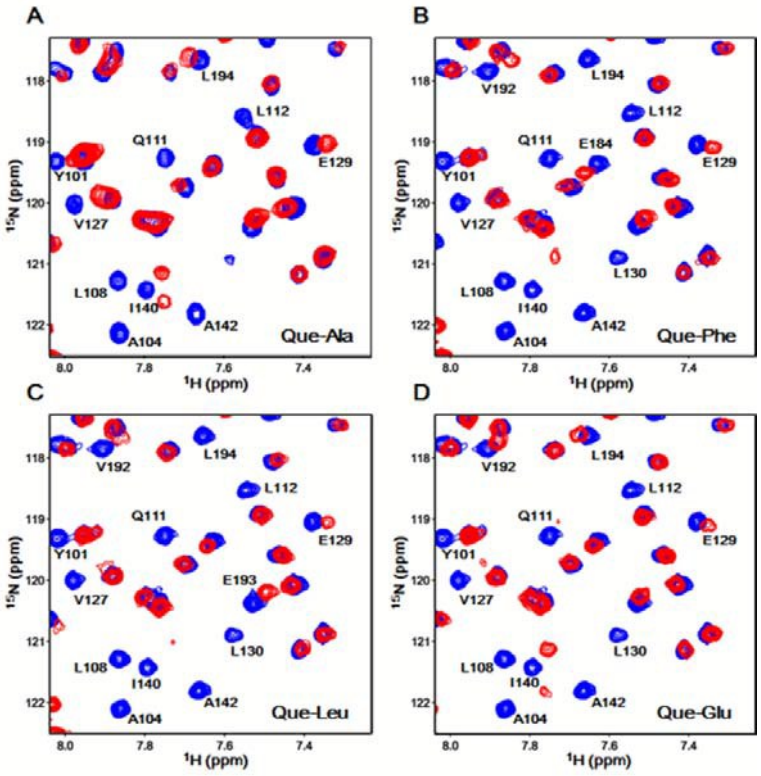

Figure 9: Mapping the Bcl-xL-quercetin binding interface by NMR. Selective region of superimposition of the $^{1}H-^{15}N$ HSQC NMR spectra of ^{15}N-labeled Bcl-xL protein without (blue crosspeaks) and with the addition of quercetin analogues (red crosspeaks).

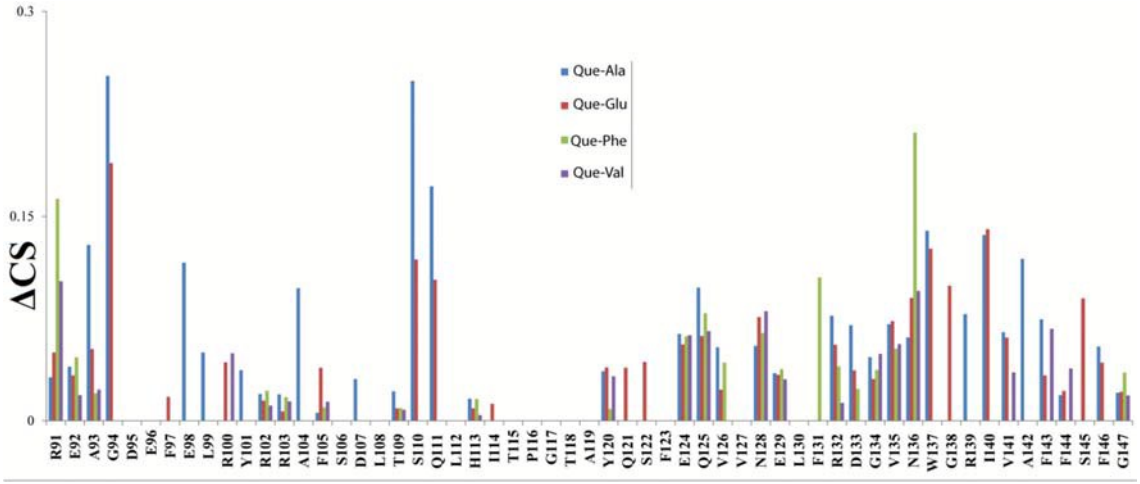

Figure 10: Chemical shift perturbation calculated using the formula $\Delta CS = [(\Delta^{1}H)^{2} + 0.2(\Delta^{15}N)^{2}]^{0.5}$ for the residues 91-147.

View Article Online
DOI: 10.1039/C7OB02045G

***In vitro* evaluation of the cytostatic and cytotoxic activity of the four quercetin-amino acid conjugates against prostate cancer cells**

To evaluate the bioactivity of the four different analogues we conducted MTT assay to determine the cytostatic and cytotoxic activity in prostate cancer cell lines. Since we would like also to evaluate the differential impact of the hPEPT1 transporters on the activity of quercetin-aminoacid conjugates we rationally selected DU-145 and PC-3 prostate cancer cell lines. This, since it has been determined that PC-3 overexpress hPEPT1, in contrast to the DU-145 cell line which possess very low levels of hPEPT1 expression[22]. Therefore, and according to our hypothesis we should expect that the four analogues should present more enhanced activity in the PC-3 cell line, overexpressing the hPEPT1, in contrast to DU-145, and thus lead to higher intracellular delivery of the conjugates. In Table 7 are presented the recorded values. It is evident that all analogues illustrated consistently the highest values in the PC-3 cell line in contrast to the DU-145 cell line. Que-Glu and Que-Ala exhibited the lowest IG50 values against PC-3 cells, while Que-Leu and Que-Phe were found active but with lower cytostatic potency. It is interesting that Que-Glu presented an IG50 value (6±0.98 μM) in PC-3 cells 17-fold lower with respect to the relevant value in DU-145 cells. These results corroborate to the fact that the quercetin – aminoacid conjugates operate better in the PC-3 cell line possibly due to the overexpression of the human peptide transporter hPEPT1 recognizing and transporting them in the cell interior.

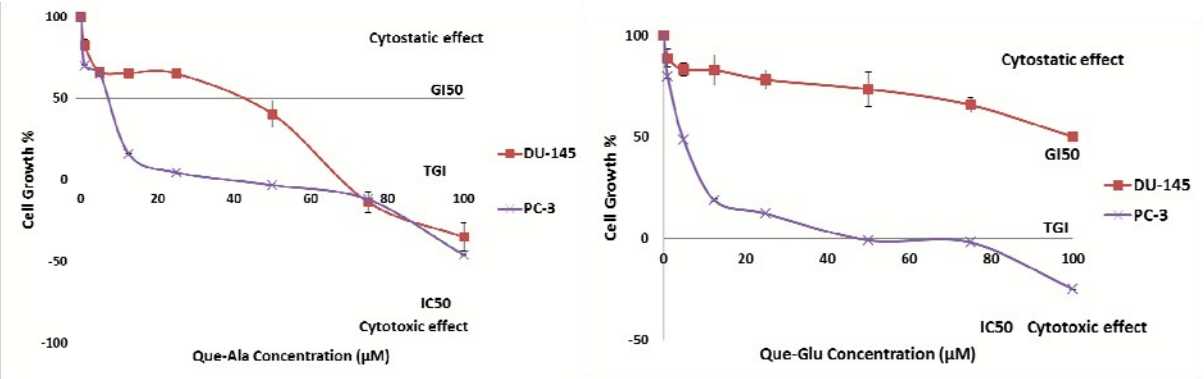

View Article Online
DOI: 10.1039/C7OB02045G

Figure 11. Growth inhibition (sensitivity curves) of DU-145 and PC-3 cells, produced after treatment with Que-Ala, Que-Glu, Que-Leu, Que-Phe.

Table 7. Growth inhibition/cytostatic (GI50 and TGI μM) and cytocidal/cytotoxic (IC50 μM) anticancer effects induced by Que-Ala, Que-Leu, Que-Glu and Que-Phe on DU-145 and PC-3 human cancer prostate cell lines.

Human prostate cell lines	Que-Ala			Que-Glu			Que-Leu			Que-Phe		
	GI50*	TGI*	IC50*	GI50*	TGI*	IC50*	GI50*	TGI*	IC50*	GI50*	TGI*	IC50*
DU-145 *(non-expressing hPEPT1)*	42±4.11	68±3.78	>100	100±2.63	>100	>100	50±3.05	>100	>100	58±8.2	>100	>100
PC-3 *(over-expressing hPEPT1)*	7±1.07	36±1.42	100±2.31	6±0.98	44±1.24	>100	28±1.34	44±1.28	99±1.10	27±0.80	58±1.02	>100

* mean±SD (μM) derived from triplicate experiment

Conclusions

Tailoring compounds to interact with anti-apoptotic proteins such Bcl-xL is a long quest given their importance as anticancer agents. The chemical space to rationally design compounds able to interact with this protein is not fully characterized and the discovery of new hits is highly desirable. Natural products can shape a good starting point to develop more potent compounds since they are evolutionary pre-validated ligands for numerous protein targets. Herein, IFD calculations and MD simulations were exploited to rationally design quercetin analogues to target Bcl-xL. Quercetin was conjugated with four amino acids (alanine, glutamic acid, phenylalanine and leucine) on ring B. The new analogs were designed to ameliorate the lipophilicity drawback of quercetin, increase its binding profile capacity for Bcl-xL and enhance their selectivity for cancer cell lines overexpressing peptide transporters as have been utilized for other drug-amino acid conjugates. This was evidenced through docking calculations in the Bcl-xL protein indicating that they bind in the BH3 binding site. MD simulations showed that the formed interactions with crucial residues of the protein are stable in time. MM-PBSA and MM-GBSA showed that the Que-Glu3 displays the highest binding affinity (-47.16 kcal/mol). 2D NMR chemical shift perturbation mapping pinpointed that the analogues cause chemical shift changes mainly in the residues of the BH3 binding groove, thus confirming the *in silico* studies. Fluorescence data were also in

View Article Online
DOI: 10.1039/C7OB02045G

accordance to the *in* silico and NMR studies. Cytostatic evaluation of the different quercetin conjugates was conducted in two different prostate cancer cell lines, PC-3, overexpressing the peptide transporter hPEPT1 and DU-145, presenting very low expression levels of this transporter. An enhanced bioactivity was consistently recorded for all analogues in PC-3 and it is worth mentioning that Que-Glu presented a 17-fold lower IG50 value in PC-3 cells with respect to DU-145. Thus, flavonoid prodrugs conjugated with amino acids could be a viable approach to enhance their pharmaceutic window.

Authors contribution Project conception: AGT, TM; Experimental design: AGT, TK, TM NMR data acquisition: EV, NS, AT, MSL, SWC; MS data acquisition: ES; ITC data acquisition and analysis: MC, AGT; Fluorescence spectroscopy data acquisition and analysis: MC, AGT; Synthesis: NS, EV, AT; Cell cultures: EG, GG; Data analysis: AGT, MC, TK, SWC, MSL, EG, GG; Manuscript preparation: AGT, TK, TM, MC.

Acknowledgments

This work was co-financed by the European Union (European Social Fund – ESF) and Greek national funds through the Operational Program "Education and Lifelong Learning" of the National Strategic Reference Framework (NSRF) - Research Funding Program: ARISTEIA II. Investing in knowledge society through the European Social Fund. Additionally, it was supported by the NRF grant funded by the Korea government (MEST) (NRF-2014R1A2A2A05002961; to SWC).

References

1. Youle, R. J.; Strasser, A., The BCL-2 protein family: Opposing activities that mediate cell death. *Nat. Rev. Mol. Cell Biol.* **2008**, 9, 47-59.
2. Levine, B.; Sinha, S.; Kroemer, G., Bcl-2 family members: Dual regulators of apoptosis and autophagy. *Autophagy* **2008**, 4, 600-606.
3. Kirkin, V.; Joos, S.; Zörnig, M., The role of Bcl-2 family members in tumorigenesis. *Biochim. Biophys. Acta* **2004**, 1644, 229-249.
4. Petros, A. M.; Olejniczak, E. T.; Fesik, S. W., Structural biology of the Bcl-2 family of proteins. *Biochim. Biophys. Acta* **2004**, 1644, 83-94.
5. Yip, K. W.; Reed, J. C., Bcl-2 family proteins and cancer. *Oncogene* **2008**, 27, 6398-406.
6. Lessene, G.; Czabotar, P. E.; Colman, P. M., BCL-2 family antagonists for cancer therapy. *Nat. Rev. Drug Discov.* **2008**, 7, 989-1000.

View Article Online
DOI: 10.1039/C7OB02045G

7. Westphal, D.; Kluck, R. M.; Dewson, G., Building blocks of the apoptotic pore: How Bax and Bak are activated and oligomerize during apoptosis. *Cell Death Differ.* **2014**, 21, 196-205.
8. Ku, B.; Liang, C.; Jung, J. U.; Oh, B. H., Evidence that inhibition of BAX activation by BCL-2 involves its tight and preferential interaction with the BH3 domain of BAX. *Cell Res.* **2011**, 21, 627-641.
9. Liu, X.; Dai, S.; Zhu, Y.; Marrack, P.; Kappler, J. W., The structure of a Bcl-xL/Bim fragment complex: Implications for Bim function. *Immunity* **2003**, 19, 341-352.
10. Shimizu, S.; Eguchi, Y.; Kosaka, H.; Kamiike, W.; Matsuda, H.; Tsujimoto, Y., Prevention of hypoxia-induced cell death by Bcl-2 and Bcl-xL. *Nature* **1995**, 374, 811-813.
11. Muchmore, S. W.; Sattler, M.; Liang, H.; Meadows, R. P.; Harlan, J. E.; Yoon, H. S.; Nettesheim, D.; Chang, B. S.; Thompson, C. B.; Wong, S. L.; Ng, S. C.; Fesik, S. W., X-ray and NMR structure of human Bcl-xL, an inhibitor of programmed cell death. *Nature* **1996**, 381, 335-341.
12. Sattler, M.; Liang, H.; Nettesheim, D.; Meadows, R. P.; Harlan, J. E.; Eberstadt, M.; Yoon, H. S.; Shuker, S. B.; Chang, B. S.; Minn, A. J.; Thompson, C. B.; Fesik, S. W., Structure of Bcl-x(L)-Bak peptide complex: Recognition between regulators of apoptosis. *Science* **1997**, 275, 983-986.
13. Volkmann, N.; Marassi, F. M.; Newmeyer, D. D.; Hanein, D., The rheostat in the membrane: BCL-2 family proteins and apoptosis. *Cell Death Differ.* **2014**, 21, 206-215.
14. Roy, M. J.; Vom, A.; Czabotar, P. E.; Lessene, G., Cell death and the mitochondria: therapeutic targeting of the BCL-2 family-driven pathway. *British journal of pharmacology* **2014**, 171, 1973-87.
15. Scott, D. E.; Bayly, A. R.; Abell, C.; Skidmore, J., Small molecules, big targets: Drug discovery faces the protein-protein interaction challenge. *Nature Reviews Drug Discovery* **2016**, 15, 533-550.
16. Arkin, M. R.; Tang, Y.; Wells, J. A., Small-molecule inhibitors of protein-protein interactions: Progressing toward the reality. *Chem. Biol.* **2014**, 21, 1102-1114.
17. Tzakos, A. G.; Fokas, D.; Johannes, C.; Moussis, V.; Hatzimichael, E.; Briasoulis, E., Targeting oncogenic protein-protein interactions by diversity oriented synthesis and combinatorial chemistry approaches. *Molecules* **2011**, 16, 4408-27.
18. Tam, C. S.; Seymour, J. F.; Roberts, A. W., Progress in BCL2 inhibition for patients with chronic lymphocytic leukemia. *Semin. Oncol.* **2016**, 43, 274-9.
19. Milroy, L. G.; Grossmann, T. N.; Hennig, S.; Brunsveld, L.; Ottmann, C., Modulators of protein-protein interactions. *Chem. Rev.* **2014**, 114, 4695-748.
20. Primikyri, A.; Chatziathanasiadou, M. V.; Karali, E.; Kostaras, E.; Mantzaris, M. D.; Hatzimichael, E.; Shin, J. S.; Chi, S. W.; Briasoulis, E.; Kolettas, E.; Gerothanassis, I. P.; Tzakos, A. G., Direct binding of Bcl-2 family proteins by quercetin triggers its pro-apoptotic activity. *ACS Chem. Biol.* **2014**, 9, 2737-41.
21. Bhutia, Y. D.; Babu, E.; Ramachandran, S.; Ganapathy, V., Amino Acid transporters in cancer and their relevance to "glutamine addiction": novel targets for the design of a new class of anticancer drugs. *Cancer Res.* **2015**, 75, 1782-8.
22. Tai, W.; Chen, Z.; Cheng, K., Expression profile and functional activity of peptide transporters in prostate cancer cells. *Mol Pharm* **2013**, 10, 477-87.
23. Meredith, D., The mammalian proton-coupled peptide cotransporter PepT1: sitting on the transporter–channel fence? *Philosophical Transactions of the Royal Society B: Biological Sciences* **2009**, 364, 203-207.
24. Friedrichsen, G. M.; Nielsen, C. U.; Steffansen, B.; Begtrup, M., Model prodrugs designed for the intestinal peptide transporter. A synthetic approach for coupling of hydroxy-

View Article Online
DOI: 10.1039/C7OB02045G

containing compounds to dipeptides. *European journal of pharmaceutical sciences : official journal of the European Federation for Pharmaceutical Sciences* **2001**, 14, 13-9.
25. Kwak, E. Y.; Shim, W. S.; Chang, J. E.; Chong, S.; Kim, D. D.; Chung, S. J.; Shim, C. K., Enhanced intracellular accumulation of a non-nucleoside anti-cancer agent via increased uptake of its valine ester prodrug through amino acid transporters. *Xenobiotica* **2012**, 42, 603-13.
26. Huttunen, K. M.; Huttunen, J.; Aufderhaar, I.; Gynther, M.; Denny, W. A.; Spicer, J. A., L-Type amino acid transporter 1 (lat1)-mediated targeted delivery of perforin inhibitors. *Int. J. Pharm.* **2016**, 498, 205-16.
27. Gynther, M.; Laine, K.; Ropponen, J.; Leppanen, J.; Mannila, A.; Nevalainen, T.; Savolainen, J.; Jarvinen, T.; Rautio, J., Large neutral amino acid transporter enables brain drug delivery via prodrugs. *J. Med. Chem.* **2008**, 51, 932-6.
28. Prati, F.; Goldman-Pinkovich, A.; Lizzi, F.; Belluti, F.; Koren, R.; Zilberstein, D.; Bolognesi, M. L., Quinone-amino acid conjugates targeting Leishmania amino acid transporters. *PLoS One* **2014**, 9, e107994.
29. Ninomiya, M.; Tanaka, K.; Tsuchida, Y.; Muto, Y.; Koketsu, M.; Watanabe, K., Increased bioavailability of tricin-amino acid derivatives via a prodrug approach. *J Med Chem* **2011**, 54, 1529-36.
30. Kim, M. K.; Park, K. S.; Yeo, W. S.; Choo, H.; Chong, Y., In vitro solubility, stability and permeability of novel quercetin-amino acid conjugates. *Bioorganic & medicinal chemistry* **2009**, 17, 1164-71.
31. Charisiadis, P.; Primikyri, A.; Exarchou, V.; Tzakos, A.; Gerothanassis, I. P., Unprecedented Ultra-High-Resolution Hydroxy Group 1H NMR Spectroscopic Analysis of Plant Extracts. *J. Nat. Prod.* **2011**, 74, 2462-2466.
32. Biasutto, L.; Marotta, E.; De Marchi, U.; Zoratti, M.; Paradisi, C., Ester-based precursors to increase the bioavailability of quercetin. *J. Med. Chem.* **2007**, 50, 241-53.
33. Rawel, H. M.; Frey, S. K.; Meidtner, K.; Kroll, J.; Schweigert, F. J., Determining the binding affinities of phenolic compounds to proteins by quenching of the intrinsic tryptophan fluorescence. *Mol. Nutr. Food Res.* **2006**, 50, 705-13.
34. Epps, D. E.; Raub, T. J.; Caiolfa, V.; Chiari, A.; Zamai, M., Determination of the affinity of drugs toward serum albumin by measurement of the quenching of the intrinsic tryptophan fluorescence of the protein. *J. Pharm. Pharmacol.* **1999**, 51, 41-8.
35. Madhavi Sastry, G.; Adzhigirey, M.; Day, T.; Annabhimoju, R.; Sherman, W., Protein and ligand preparation: Parameters, protocols, and influence on virtual screening enrichments. *J. Comput.-Aided Mol. Des.* **2013**, 27, 221-234.
36. Olsson, M. H. M.; Søndergaard, C. R.; Rostkowski, M.; Jensen, J. H., PROPKA3: Consistent treatment of internal and surface residues in empirical p K a predictions. *J. Chem. Theory Comput.* **2011**, 7, 525-537.
37. Shivakumar, D.; Williams, J.; Wu, Y.; Damm, W.; Shelley, J.; Sherman, W., Prediction of Absolute Solvation Free Energies using Molecular Dynamics Free Energy Perturbation and the OPLS Force Field. *J. Chem. Theory Comput.* **2010**, 6, 1509-1519.
38. Fosgerau, K.; Hoffmann, T., Peptide therapeutics: current status and future directions. *Drug Discovery Today* **2015**, 20, 122-128.
39. Cordoba-Chacon, J.; Gahete, M. D.; Culler, M. D.; Castano, J. P.; Kineman, R. D.; Luque, R. M., Somatostatin dramatically stimulates growth hormone release from primate somatotrophs acting at low doses via somatostatin receptor 5 and cyclic AMP. *Journal of neuroendocrinology* **2012**, 24, 453-63.
40. Pastor-Anglada, M.; Pérez-Torras, S., Nucleoside transporter proteins as biomarkers of drug responsiveness and drug targets. *Frontiers in Pharmacology* **2015**, 6, 13.

View Article Online
DOI: 10.1039/C7OB02045G

41. Sherman, W.; Beard, H. S.; Farid, R., Use of an induced fit receptor structure in virtual screening. *Chem. Biol. Drug Des.* **2006**, 67, 83-84.
42. Sherman, W.; Day, T.; Jacobson, M. P.; Friesner, R. A.; Farid, R., Novel procedure for modeling ligand/receptor induced fit effects. *J. Med. Chem.* **2006**, 49, 534-553.
43. Lee, E. F.; Czabotar, P. E.; Smith, B. J.; Deshayes, K.; Zobel, K.; Colman, P. M.; Fairlie, W. D., Crystal structure of ABT-737 complexed with Bcl-xL: Implications for selectivity of antagonists of the Bcl-2 family [1]. *Cell Death Differ.* **2007**, 14, 1711-1713.
44. Lessene, G.; Czabotar, P. E.; Sleebs, B. E.; Zobel, K.; Lowes, K. N.; Adams, J. M.; Baell, J. B.; Colman, P. M.; Deshayes, K.; Fairbrother, W. J.; Flygare, J. A.; Gibbons, P.; Kersten, W. J. A.; Kulasegaram, S.; Moss, R. M.; Parisot, J. P.; Smith, B. J.; Street, I. P.; Yang, H.; Huang, D. C. S.; Watson, K. G., Structure-guided design of a selective BCL-XL inhibitor. *Nat. Chem. Biol.* **2013**, 9, 390-397.
45. Zhou, H.; Chen, J.; Meagher, J. L.; Yang, C. Y.; Aguilar, A.; Liu, L.; Bai, L.; Cong, X.; Cai, Q.; Fang, X.; Stuckey, J. A.; Wang, S., Design of Bcl-2 and Bcl-xL inhibitors with subnanomolar binding affinities based upon a new scaffold. *J. Med. Chem.* **2012**, 55, 4664-4682.
46. Sleebs, B. E.; Czabotar, P. E.; Fairbrother, W. J.; Fairlie, W. D.; Flygare, J. A.; Huang, D. C. S.; Kersten, W. J. A.; Koehler, M. F. T.; Lessene, G.; Lowes, K.; Parisot, J. P.; Smith, B. J.; Smith, M. L.; Souers, A. J.; Street, I. P.; Yang, H.; Baell, J. B., Quinazoline sulfonamides as dual binders of the proteins B-cell lymphoma 2 and B-cell lymphoma extra long with potent proapoptotic cell-based activity. *J. Med. Chem.* **2011**, 54, 1914-1926.
47. Schroeder, G. M.; Wei, D.; Banfi, P.; Cai, Z. W.; Lippy, J.; Menichincheri, M.; Modugno, M.; Naglich, J.; Penhallow, B.; Perez, H. L.; Sack, J.; Schmidt, R. J.; Tebben, A.; Yan, C.; Zhang, L.; Galvani, A.; Lombardo, L. J.; Borzilleri, R. M., Pyrazole and pyrimidine phenylacylsulfonamides as dual Bcl-2/Bcl-xL antagonists. *Bioorg. Med. Chem. Lett.* **2012**, 22, 3951-3956.
48. Brady, R. M.; Vom, A.; Roy, M. J.; Toovey, N.; Smith, B. J.; Moss, R. M.; Hatzis, E.; Huang, D. C. S.; Parisot, J. P.; Yang, H.; Street, I. P.; Colman, P. M.; Czabotar, P. E.; Baell, J. B.; Lessene, G., De-novo designed library of benzoylureas as inhibitors of BCL-X L: Synthesis, structural and biochemical characterization. *J. Med. Chem.* **2014**, 57, 1323-1343.
49. Smith, B. J.; Lee, E. F.; Checco, J. W.; Evangelista, M.; Gellman, S. H.; Fairlie, W. D., Structure-Guided Rational Design of α/β-Peptide Foldamers with High Affinity for BCL-2 Family Prosurvival Proteins. *ChemBioChem* **2013**, 14, 1564-1572.
50. Lee, E. F.; Czabotar, P. E.; Yang, H.; Sleebs, B. E.; Lessene, G.; Colman, P. M.; Smith, B. J.; Fairlie, W. D., Conformational changes in Bcl-2 pro-survival proteins determine their capacity to bind ligands. *J. Biol. Chem.* **2009**, 284, 30508-30517.
51. Salomon-Ferrer, R.; Gotz, A. W.; Poole, D.; Le Grand, S.; Walker, R. C., Routine Microsecond Molecular Dynamics Simulations with AMBER on GPUs. 2. Explicit Solvent Particle Mesh Ewald. *J. Chem. Theory Comput.* **2013**, 9, 3878-88.
52. Le Grand, S.; Götz, A. W.; Walker, R. C., SPFP: Speed without compromise - A mixed precision model for GPU accelerated molecular dynamics simulations. *Comput. Phys. Commun.* **2013**, 184, 374-380.
53. Case, D. A.; Cheatham Iii, T. E.; Darden, T.; Gohlke, H.; Luo, R.; Merz Jr, K. M.; Onufriev, A.; Simmerling, C.; Wang, B.; Woods, R. J., The Amber biomolecular simulation programs. *J. Comput. Chem.* **2005**, 26, 1668-1688.
54. Case, D.; Darden, T. A.; Cheatham, T. E.; Simmerling, C.; Wang, J.; Duke, R.; Luo, R.; Crowley, M.; Walker, R.; Zhang, W.; Merz, K. M.; Wang, B.; Hayik, S.; Roitberg, A.; Seabra, G.; Kolossváry, I.; Wong, K. F.; Paesani, F.; Vanicek, J.; Wu, X.; Brozell, S.; Steinbrecher, T.; Gohlke, H.; Yang, L.; Tan, C.; Mongan, J.; Hornak, V.; Cui, G.; Mathews,

View Article Online
DOI: 10.1039/C7OB02045G

D. H.; Seetin, M. G.; Sagui, C.; Babin, V.; Kollman, P., *AMBER 12, University of California, San Francisco.* 2012.

55. Frisch, M. J.; Trucks, G. W.; Schlegel, H. B.; Scuseria, G. E.; Robb, M. A.; Cheeseman, J. R.; Scalmani, G.; Barone, V.; Mennucci, B.; Petersson, G. A.; Nakatsuji, H.; Caricato, M.; Li, X.; Hratchian, H. P.; Izmaylov, A. F.; Bloino, J.; Zheng, G.; Sonnenberg, J. L.; Hada, M.; Ehara, M.; Toyota, K.; Fukuda, R.; Hasegawa, J.; Ishida, M.; Nakajima, T.; Honda, Y.; Kitao, O.; Nakai, H.; Vreven, T.; Montgomery Jr., J. A.; Peralta, J. E.; Ogliaro, F.; Bearpark, M. J.; Heyd, J.; Brothers, E. N.; Kudin, K. N.; Staroverov, V. N.; Kobayashi, R.; Normand, J.; Raghavachari, K.; Rendell, A. P.; Burant, J. C.; Iyengar, S. S.; Tomasi, J.; Cossi, M.; Rega, N.; Millam, N. J.; Klene, M.; Knox, J. E.; Cross, J. B.; Bakken, V.; Adamo, C.; Jaramillo, J.; Gomperts, R.; Stratmann, R. E.; Yazyev, O.; Austin, A. J.; Cammi, R.; Pomelli, C.; Ochterski, J. W.; Martin, R. L.; Morokuma, K.; Zakrzewski, V. G.; Voth, G. A.; Salvador, P.; Dannenberg, J. J.; Dapprich, S.; Daniels, A. D.; Farkas, Ö.; Foresman, J. B.; Ortiz, J. V.; Cioslowski, J.; Fox, D. J. *Gaussian 09*, Gaussian, Inc.: Wallingford, CT, USA, 2009.

56. Wang, J.; Wolf, R. M.; Caldwell, J. W.; Kollman, P. A.; Case, D. A., Development and testing of a general Amber force field. *J. Comput. Chem.* **2004**, 25, 1157-1174.

57. Bayly, C. I.; Cieplak, P.; Cornell, W. D.; Kollman, P. A., A well-behaved electrostatic potential based method using charge restraints for deriving atomic charges: The RESP model. *J. Phys. Chem.* **1993**, 97, 10269-10280.

58. Izaguirre, J. A.; Catarello, D. P.; Wozniak, J. M.; Skeel, R. D., Langevin stabilization of molecular dynamics. *J. Chem. Phys.* **2001**, 114, 2090-2098.

59. Ryckaert, J. P.; Ciccotti, G.; Berendsen, H. J. C., Numerical integration of the cartesian equations of motion of a system with constraints: molecular dynamics of n-alkanes. *J. Comput. Phys.* **1977**, 23, 327-341.

60. Roe, D. R.; Cheatham, T. E., PTRAJ and CPPTRAJ: Software for processing and analysis of molecular dynamics trajectory data. *J. Chem. Theory Comput.* **2013**, 9, 3084-3095.

61. Miller, B. R.; McGee, T. D.; Swails, J. M.; Homeyer, N.; Gohlke, H.; Roitberg, A. E., MMPBSA.py: An efficient program for end-state free energy calculations. *J. Chem. Theory Comput.* **2012**, 8, 3314-3321.

62. Kollman, P. A.; Massova, I.; Reyes, C.; Kuhn, B.; Huo, S.; Chong, L.; Lee, M.; Lee, T.; Duan, Y.; Wang, W.; Donini, O.; Cieplak, P.; Srinivasan, J.; Case, D. A.; Cheatham Iii, T. E., Calculating structures and free energies of complex molecules: Combining molecular mechanics and continuum models. *Acc. Chem. Res.* **2000**, 33, 889-897.

63. Gohlke, H.; Kiel, C.; Case, D. A., Insights into protein-protein binding by binding free energy calculation and free energy decomposition for the Ras-Raf and Ras-RalGDS complexes. *J. Mol. Biol.* **2003**, 330, 891-913.

64. Wang, W.; Kollman, P. A., Computational study of protein specificity: The molecular basis of HIV-1 protease drug resistance. *Proc. Natl. Acad. Sci. U. S. A.* **2001**, 98, 14937-14942.

65. Mosmann, T., Rapid colorimetric assay for cellular growth and survival: application to proliferation and cytotoxicity assays. *Journal of immunological methods* **1983**, 65, 55-63.

66. Guo, Z.; Thorarensen, A.; Che, J.; Xing, L., Target the More Druggable Protein States in a Highly Dynamic Protein-Protein Interaction System. *J. Chem. Inf. Model.* **2016**, 56, 35-45.

67. Novak, W.; Wang, H.; Krilov, G., Role of protein flexibility in the design of Bcl-X(L) targeting agents: insight from molecular dynamics. *J. Comput. Aided Mol. Des.* **2009**, 23, 49-61.

View Article Online
DOI: 10.1039/C7OB02045G

68. Rutkowska, E.; Pajak, K.; Jozwiak, K., Lipophilicity--methods of determination and its role in medicinal chemistry. *Acta poloniae pharmaceutica* **2013**, 70, 3-18.

View Article Online
DOI: 10.1039/C7OB02045G

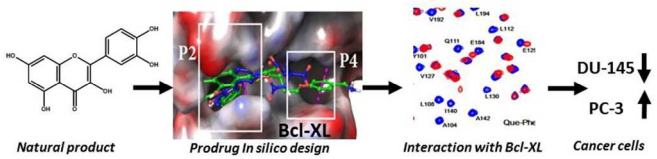

338x190mm (96 x 96 DPI)